Kinetic Drawbacks of Combining Electrochemical CO_2 Sorbent Reactivation with CO_2 Absorption

Jonathan Boualavong and Christopher A. Gorski*

Department of Civil & Environmental Engineering, Pennsylvania State University, University Park, Pennsylvania 16802, United States

E-mail: cag981@psu.edu

Abstract

Electrochemical CO_2 capture approaches, where electrochemical reactions control the sorbent's CO_2 affinity to drive subsequent CO_2 ab-/desorption, have gained substantial attention due to their low energy demands compared to temperature-swing approaches. Typically, the process uses separate electrochemical and mass transfer steps, producing a 4-stage (cathodic/anodic, absorption/desorption) process, but recent work proposed that these energy demands can be further reduced by combining the electrochemical and CO_2 mass transfer reactor units. Here, we used computational models to examine the practical benefit of combining electrochemical sorbent reactivation with CO_2 absorption due to this combination's implicit assumptions about the process rate, and therefore the reactor size and cost. Comparing the minimum energy demand and process time of this combined reactor to those of the separated configuration, we found that the combined absorber can reduce the energy demand by up to 67%, but doing so can also increase the process time by several orders of magnitude.

In contrast, optimizing the solution chemistry could benefit both the energy demand and process time simultaneously.

Keywords

CO_2 sorbent, process simulation, CO_2 absorption, electrochemical systems

1 Introduction

In order to avoid the worst impacts of climate change, carbon capture technologies are essential.[1–5] These technologies separate CO_2 from gaseous mixtures, creating a CO_2-depleted lean gas product released into the atmosphere and a pure CO_2 product for CO_2 utilization or storage. The most common and industrially proven approach absorbs CO_2 from a gaseous mixture into a liquid sorbent at low temperatures. After CO_2 absorption, the sorbent is heated to release high purity gaseous CO_2.[5–8] While mature, carbon capture processes driven by temperature swings are too expensive for widespread use due (*a*) to the high energy requirement for driving the process and (*b*) the high capital cost, most of which is associated with constructing the absorber column.[5,7,9–13]

Recent work on electrochemical carbon capture processes, which replace thermal energy inputs with electrical energy inputs, have been shown to have lower thermodynamic minimum energy demands across a variety of fundamental chemistries,[14–17] albeit with difficult-to-compare rates and low experimental energy efficiencies. Typically, electrochemical CO_2 capture processes use a 4-stage cycle: (*stage 1*) CO_2 is absorbed into the liquid sorbent; (*stage 2*) the sorbent is inactivated via electrochemical reactions, destabilizing the sorbent-CO_2 bond; (*stage 3*) CO_2 is released to the gas phase; and (*stage 4*) the sorbent is reactivated via electrochemical reactions, restoring its affinity for CO_2. This 4-stage cycle makes distinct the electrochemical reactions from the CO_2 transfer processes to make it easier to design and study: each stage, and thus each reactor, only has one process being intentionally driven at

a time. Despite low minimum energy demands for electrochemical CO_2 capture, bench-scale energy demands are still greater than established CO_2 capture design targets due to poor energy efficiencies[13,16,18–25] and unoptimized sorbent chemistries.[17]

To further reduce the energy demands of electrochemical carbon capture, multiple research groups have proposed a reactor configuration where the electrochemical half cells are combined with their subsequent CO_2 transfer units;[14,15] *i.e.*, sorbent inactivation is combined with CO_2 release (*stages 2 and 3*) and sorbent reactivation is combined with CO_2 absorption (*stages 4 and 1*). By combining the two processes, the minimum energy demand is predicted to decrease by approximately 60-70%, with approximately $\frac{2}{3}$ of the decrease coming from combining absorption with sorbent reactivation.[15] This improvement is made possible by the reduction in the CO_2 concentration difference across the electrochemical cell: the simultaneous absorption and desorption of CO_2 prevents the CO_2 partial pressure from decreasing below the inlet pressure or increasing above the outlet pressure during the electrochemical process. With a smaller CO_2 concentration difference across the electrochemical cell, the minimum cell voltage will decrease, reducing the energy required for the electrochemical reaction. We note, however, that to our knowledge, these combined configurations have only been theorized at industrial scales, and practical considerations, such as what these cells would actually look like and whether they can even achieve the proposed energy benefits, have not been fully discussed in the literature.

One important practical consideration is that the energy benefit of the combined absorber and combined desorber relies on the implicit assumption that the CO_2 mass transport rate must be sufficiently fast that it can be treated as instantaneous compared to the rate of the electrochemical reaction. If the opposite were true, the electrochemical reaction would proceed to completion prior to the transport of any CO_2, which is effectively identical to a 4-stage process in which electrochemical inactivation/reactivation stages (*stages 2 and 4*) intentionally precedes CO_2 desorption/absorption (*stage 3 and 1*), respectively. Given that the CO_2 absorption reaction is often the rate-limiting step of a CO_2 capture process[6,12,13,26]

and that the majority of the energy benefit is observed when combining the absorber with sorbent reactivation, we explored the trade-off between the energy demand and the capture rate when combining stages (*1*) and (*4*). We specifically hypothesized that the requirement of operating at current densities slower than the CO_2 absorption rate would cause the process time to be unusable, even when accounting for the improvements to the energy demand. Here, we defined an "unusable" process time as requiring substantially greater liquid residence times than those required in the temperature swing carbon capture process. Given the absorber's large contribution to the overall cost,[13] compensating for the greater liquid residence time with a larger absorber would negate the cost benefits from reducing the energy demand.

We tested this hypothesis using a computational model of carbon capture driven by pH swings created by aqueous-phase proton-coupled electron transfers. This is a widely used and studied electrochemical carbon capture approach that is simple to model compared to other electrochemical CO_2 capture mechanisms.[14,27–30] During this process, the reduction of the redox-active molecule, most commonly a substituted quinone (Q) in an aqueous electrolyte, is coupled to the uptake of a proton from solution, leading to an increase in the pH (Eq. 1). Because CO_2 in aqueous solutions exists in equilibrium with carbonic acid, pH changes lead to increases in the total dissolved inorganic carbon ($\mathrm{DIC} = [H_2CO_3] + [HCO_3^-] + [CO_3^{2-}]$). As a result, electrochemical reduction drives CO_2 absorption via the production of hydroxide ions, a strong CO_2 sorbent, while oxidation leads to hydroxide ion consumption and CO_2 release.

$$\mathrm{Q} + 2\mathrm{H}^+ + 2\mathrm{e}^- \leftrightarrow \mathrm{QH}_2 \tag{1}$$

We expanded existing computational aqueous chemistry models of this electrochemical process,[14,17] which model the 4-stage configuration with separated unit operations, to also model the process in which electrochemical sorbent reactivation (*stage 4*) and CO_2 absorption (*stage 1*) are combined, henceforth referred to as a "combined absorber" configuration.

While electrochemical CO_2 capture has been demonstrated using solid phase moieties that can uptake protons upon electrochemical reduction (heterogeneous sorbents),[23] we limit ourselves to the homogeneous process to be consistent with existing computational models of electrochemical CO_2 capture. We identified changes to the idealized physical limits of the energy demand and process time as a function of the reactor configurations across the solution chemistry and operating condition parameter space by using an adaptive sampling approach.[17] This study design allowed us to discern how the decrease in energy demand and increase in absorber liquid residence time changed as a result of chemical process design decisions. By considering the idealized energy and rate behavior, this work sought to eliminate from consideration the solution chemistries and operating conditions that can never achieve the energy or process time targets when using a particular reactor configuration. While the set of viable process conditions will be smaller than those reported here due to, for instance, energy inefficiencies, this computational analysis helps reduce the parameter space of future experimental studies to a more feasible scope. Specifically, we identified the conditions in which optimizing the solution chemistry would be more appropriate than redesigning the absorber to perform both CO_2 absorption and electrochemical sorbent reactivation. While this study investigated one specific electrochemical carbon capture process, we expect the general trend of reducing the minimum energy demand and increasing the requisite absorber liquid residence time to be true for most other electrochemical carbon capture mechanisms, although the magnitude of these effects will depend on the mechanism's specific physical properties and realistic chemical constraints.

2 Methods

2.1 Model Description and Assumptions

We used a thermodynamic process model of the electrochemical pH-swing system for carbon capture as previously described (Eq. 2-7).[14,17] This model simulates how the concentra-

tions of different species change over the course of the electrochemical CO_2 capture process, and these concentrations are then used in both our energy demand and process time estimates. Briefly, in this chemical process, carbon capture is driven by proton-coupled electron transfers such that electrochemical reduction leads to an increase in the solution pH and a corresponding increase in the CO_2 absorption capacity, and electrochemical oxidation causes the reverse. This process assumes the direct binding between the deprotonated reduced hydroquinone (Q^{2-}) and CO_2 is insignificant because this reaction has not been observed in protic solvents, and the carbonic acid chemistry (Eqs. 2, 5-6) explicitly assumes the solvent is water.[31–33] For the 4-stage configuration with separated unit operations, we simulated the electrochemical unit operations of oxidative sorbent inactivation and reductive sorbent reactivation (*stages 2 and 4*) by changing the state of charge, y_r (Eq. 8), *i.e.*, the fraction of the redox-active molecule in the reduced state, at constant total dissolved inorganic carbon. To simulate the mass transport unit operations of CO_2 absorption and release (*stages 1 and 3*), we manipulated the DIC at a constant state of charge until the partial pressure would be at equilibrium with the feed gas of a coal-fired power plant ($P_{\text{feed}} = 0.15$ atm) and pure outlet gas ($P_{\text{out}} = 1$ atm) streams, respectively (Figure 1).

$$\mathrm{CO_2(g) + H_2O \rightleftharpoons H_2CO_3} \quad (2)$$

$$\mathrm{QH_2 \rightleftharpoons QH^- + H^+} \quad (3)$$

$$\mathrm{QH^- \rightleftharpoons Q^{2-} + H^+} \quad (4)$$

$$\mathrm{H_2CO_3 \rightleftharpoons HCO_3^- + H^+} \quad (5)$$

$$\mathrm{HCO_3^- \rightleftharpoons CO_3^{2-} + H^+} \quad (6)$$

$$\mathrm{H_2O \rightleftharpoons H^+ + OH^-} \quad (7)$$

$$y_r = \frac{[\mathrm{QH_2}] + [\mathrm{QH^-}] + [\mathrm{Q^{2-}}]}{[\mathrm{Q}]_{\mathrm{tot}}} \quad (8)$$

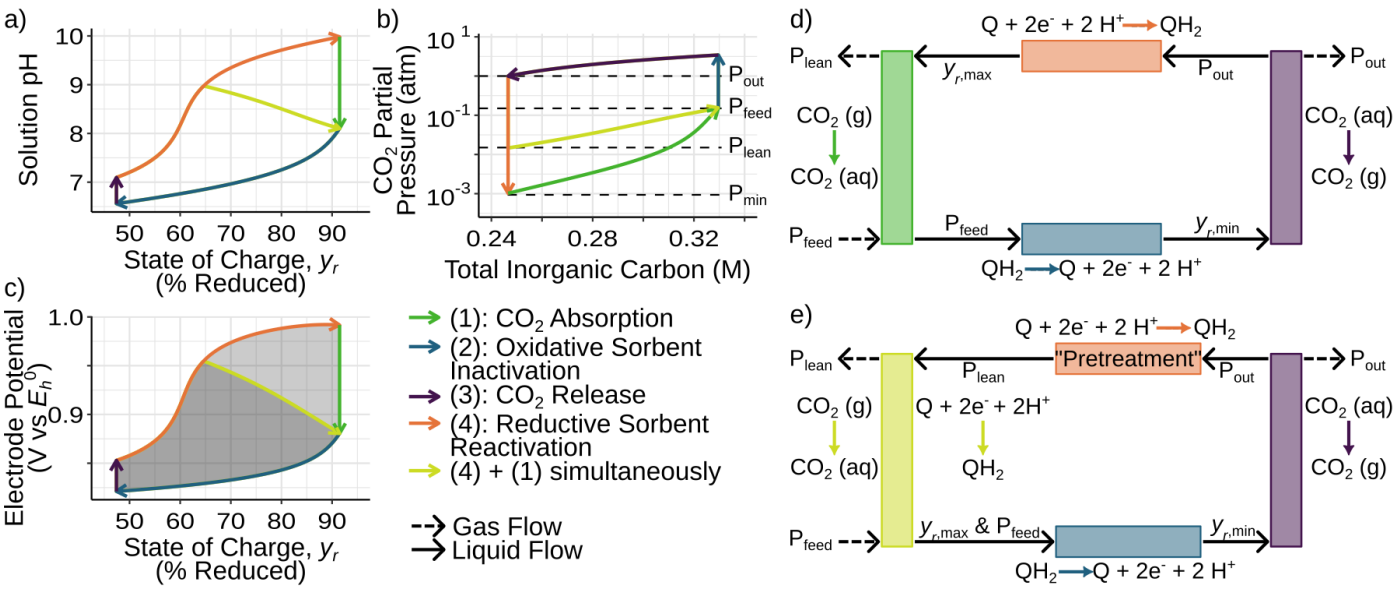

Figure 1: Example idealized thermodynamic cycle of electrochemical carbon capture, showing the most relevant process-level variables: (a) Changes to solution pH as charge is passed and (b) Changes in the CO_2 partial pressure at the vapor-liquid interface as CO_2 is absorbed and desorbed. The combined absorber process stage (Reactivation + Absorption) begins CO_2 absorption at the target lean gas pressure ($P_{\text{lean}} = 0.1P_{\text{feed}}$) and completes at the same solution chemistry composition as the unmodified CO_2 absorption stage. (c) Changes to the electrode potential (vs. the standard reduction potential, E_{h}^0 defined at pH = 0 (Eq. 9)) as charge is passed. The dark shaded region signifies the energy demand of the process with a combined absorber. The light shaded region signifies the additional energy required by the standard 4-stage process. (d) Schematic representation of the standard 4-stage process with separated unit operations and (e) the combined absorber configuration show the chemical process being targeted in each unit operation. State of charge and partial pressure values listed over the liquid flow arrows are the ending criteria for each stage.

To model the combined absorber configuration, we used the same oxidative sorbent inactivation (*2*) and CO_2 release stages (*3*), but modified the reductive sorbent reactivation (*4*) and CO_2 absorption stages (*1*). Reductive sorbent reactivation was identical to the 4-stage process until the concentration of carbonic acid in solution would be at equilibrium with the lean gas CO_2 partial pressure (P_{lean}), set at 10% of the feed gas CO_2 partial pressure. This preliminary change in the state of charge without CO2 absorption was a pretreatment step required to ensure that CO2 would be captured in the absorber, which can be achieved by having multiple electrochemical cells in series, the first of which is closed to

gas exchange (the pretreatment step) and the last of which is open to gas exchange (the combined absorber) (Figure 1e). To balance both cathodic half-cells, the oxidative sorbent inactivation step could be a single anodic half-cell electrically connected to both the cathodic pretreatment step and the combined absorber or two separate half-cells, one connected to each. Given that these sysetms are often run galvanostatically,[14,23,34,35] if there is a single anodic half-cell, the pretreatment step will be forced operate at the same low current as the combined absorber. After pretreatment, we incrementally increased both the state of charge and DIC to their final values, which were known because the final solution chemistry state was defined by the state of charge maximum and P_{lean}. We assumed that the state of charge and DIC were linearly related as a first approximation; modeling the precise, potentially nonlinear, relationship between these two variables during concerted electrochemical reduction and CO_2 absorption requires a more detailed (spatially- and temporally-resolved) CO_2 absorption model than the average CO_2 flux approximation used in this analysis (Section 2.2).

If the electrochemical pretreatment step is not performed prior to entering the counter-current mass exchanger, the typical reactor for CO_2 absorption, the concentration difference at the top of the absorber where liquid sorbent enters and the lean gas exits in would lead to local CO_2 desorption going directly into the lean gas, elevating the lean gas CO_2 concentration. This is because the liquid sorbent at this point in the process is at equilibrium with a higher CO_2 partial pressure (1 atm) than the lean gas (0.015 atm). Due to this necessary pretreatment, we found that describing this configuration as "3-stages," as it is commonly referred to in literature,[14,15] is misleading. Instead, we believe the term "combined absorber" process is a more accurate representation. Although a concurrent flow mass exchanger would not require a pretreatment step because concurrent flow means any desorbed CO_2 can still be re-absorbed into the aqueous phase later in the reactor to still achieve 90% capture at the outlet, the absorption kinetics would be slower on average.[21,26,36,37] Consequently, our combined absorber process model represents a best-case scenario that minimizes the process

time impacts, and a true 3-stage process with concurrent vapor and liquid flow would require even longer process times.

Our model implicitly assumed perfect mixing of the aqueous phase, leading to lower bound energy estimates and upper bound rate estimates. We ignored ionic strength effects to simplify the model, with the expectation that inaccuracies from this assumption would be small compared to the variance caused by the variables of interest (Section 2.4), particularly given reports of near-unity activity coefficients for small organic CO_2 sorbents.[38] While carbon capture from flue gas is often performed at 313 K, due to a lack of thermodynamic data for reactions with the redox molecules at elevated temperatures, we simulated conditions at 298 K to be consistent with existing electrochemical carbon capture literature.[14,17]

2.2 Energy Demand and Process Time Objective Functions

We used the concentrations from the thermodynamic cycle to obtain the energy demand and process time using thermodynamic and kinetic relationships. The minimum energy demand was calculated by determining the Nernst potential, E_{h}, of the anode and cathode:

$$E_{\mathrm{h}}(q) = E_{\mathrm{h}}^{0} + \frac{RT}{2F} \ln \frac{[\mathrm{Q}]}{[\mathrm{Q}^{2-}]} \tag{9}$$

where E_{h}^{0} is the standard reduction potential for the electrochemical reaction, R is the ideal gas constant, T is the absolute temperature, and F is Faraday's constant. The Nernst potentials are indirectly functions of the amount of charge passed per volume, q, via the concentrations of reduced and deprotonated oxidized species, Q and Q^{2-}, respectively. Note that this equation is also implicitly dependent on the pH of the solution because the concentration of Q^{2-} at a given state of charge changes with pH. Integrating the Nerstian cell voltage ($E_{\mathrm{h,cell}}$, Eq. 10) over q gives the amount of energy consumed per volume of solution, which, when divided by the change in DIC, gives the energy per mole of CO_2, $W_{\mathrm{CO_2}}$ (Eq. 12). Due to the large difference in the lowest and highest state of charge, when the solution

first entering the anode chamber makes contact with solution entering the cathode chamber, charge transfer between the anode and the cathode may be spontaneous ($\Delta G < 0$). We assumed none of this energy could be recovered from the system, and thus any portions of the integral that would produce energy due to spontaneous discharge were treated as if the effective cell voltage, $E^*_{\mathrm{h,cell}}$, was zero (Eq. 11); this assumption gave us a conservative overestimation of energy demand. Given that our lowest calculated energy demands approached the thermodynamic work of separation, systems with energy recovery may have a broader set of viable solution chemistries, but this should not substantially change our conclusions regarding the energy-process time trade-off of interest. We clarify that this integral gives the minimum electrical work required by the system caused by chemical differences between the anode and cathode and differs from the minimum work of separation, $W_{\mathrm{sep,min}} \approx 5.9$ kJ/mol, is the energy that would be given off if the outlet gas streams were mixed, and it sets a lower limit for the minimum electrical work required.

$$E_{\mathrm{h,cell}}(q) = E_{h,\mathrm{anode}}(q) - E_{h,\mathrm{cathode}}(q) \tag{10}$$

$$E^*_{\mathrm{h,cell}}(q) = \begin{cases} E_{\mathrm{h,cell}}(q), & \text{if } (\mathrm{DIC_{anode}} - \mathrm{DIC_{cathode}})(E_{\mathrm{h,cell}}(q)) > 0 \\ 0, & \text{else} \end{cases} \tag{11}$$

$$W_{\mathrm{CO_2}} = \frac{1}{\mathrm{DIC_{anode}} - \mathrm{DIC_{cathode}}} \int_{q=0}^{q=q_{\max}} E^*_{\mathrm{cell}} dq \tag{12}$$

While the minimum electrical energy of the electrochemical process is an incomplete description of the system in practice, it is a useful point of comparison. Additional energy from equipment, *e.g.*, pumping work, would be negligible compared to the electrochemical work.[5–7,13,39] Similarly, electrochemical inefficiencies should be similar for all electrochemical carbon capture systems in this study given the same reactor design and similar chemical mechanism, allowing us to use this minimum energy to approximate how variables of interest

would affect the process's energy demand after accounting for these inefficiencies.

The reaction kinetics of the 4-stage configuration with separated unit operations was represented by the average flux of CO_2 across the vapor-liquid interface in the absorber (J), recognizing that the rate-limiting step for CO_2 capture is the CO_2 absorption process. For this analysis, we assumed that the electrochemical system would use the existing countercurrent packed bed absorber towers used in commercial-scale CO_2 capture. In the separated unit operation configuration, this reactor would be identical to that of the heat-based process, while for the combined absorber, we assumed that the packing material would be electrically conductive to also serve as the electrode. This guarantees that there is sufficient vapor-liquid interface area (10^2-10^3 m^2 interface/m^3 reactor)[6] for the CO_2 absorption reaction to proceed to completion. This area:volume ratio is similar to or greater than the electrode area:reactor volume greater than or comparable to bench-scale experiments of electrochemical CO_2 capture using this mechanism (10^{-1}-10^3 m^2 electrode/m^3 reactor),[14,28,30] particularly considering the electrochemically active surface area of flow cells with porous electrodes has been measured to be as low as 10-20% of the electrode's total area.[40] Assuming the absorber is of this design also provides additional practical benefits: (*1*) multiple input-output kinetic models of this reactor design without explicit time or space parameters already exist and have been validated to within 5% error,[41] (*2*) we could more directly compare and benchmark electrochemical CO_2 capture to the existing heat-driven technology, particularly since it would use the same supply chain networks to connect size to cost more directly, and (*3*) this analysis has relevance for the potential retrofitting of existing heat-based systems into electrochemical capture systems.

We calculated J using the van Krevelen and Hoftijzer film model of gas absorption enhanced by a chemical reaction (Eq. 13-15), which is widely used in the literature.[6,42–51] This model assumes: the reaction starts far from equilibrium such that only the forward reaction is relevant; the bulk of the liquid and gas phases are well mixed; gas phase diffusion is fast relative to liquid phase processes; and the diffusion coefficients of CO_2 and the sorbent

are similar. Of these assumptions, all but the first should be true for packed bed absorbers using the sorbent chemistries assumed here.[6] For conditions where the reaction starts close to equilibrium, this will only occur if much less than 90% CO_2 would be captured, and we applied penalty functions to increase the process time and energy demand estimates such that these conditions would not impact our description of the low energy-low process time region (Section 2.3). While our analysis is limited by assuming this absorber type, other, often more efficient, absorber designs, such as spray-based and cross-flow contactors,[52,53] lack simple quantitative input-output descriptions and would therefore require a spatially- and temporally-resolved model that is outside the scope of this work. Additionally, most alternative designs achieve higher rates by increasing the vapor-liquid interface area through liquid phase discontinuities, which would cause substantial resistive losses in the combined absorber configuration.

$$J = ([H_2CO_3]_{V-L} - [H_2CO_3]_\infty)k_L E \tag{13}$$

$$E = \frac{\mathrm{Ha}\sqrt{A}}{\tanh(\mathrm{Ha}\sqrt{A})} \tag{14}$$

$$A = \frac{E_i - E}{E_i - 1} \tag{15}$$

In this model, $[H_2CO_3]_{V\text{-}L}$ is the concentration of CO_2 at the vapor-liquid interface at the gas inlet, $[H_2CO_3]_\infty$ is the bulk aqueous concentration at the liquid inlet, k_L is the reactor's liquid mass transfer coefficient (assumed 0.1 cm/s),[6] and E is the unitless enhancement factor. The enhancement factor was calculated from the Hatta number (Ha), the sorbent concentration, the diffusion coefficients of CO_2 ($D_{CO_2} = 0.5{*}10^{-5}$ cm^2/s)[6] and sorbent (D_s), and the rate constant (k_2) for CO_2 absorption. The model used in this work expands upon prior electrochemical carbon capture models with both energy and rate estimates[17] by ex-

plicitly representing the two possible absorption reactions:

$$OH^- + CO_2 \xrightarrow{k_{2,OH}} HCO_3^- \tag{16}$$

$$H_2O + H_nQ^{n-2} + CO_2 \xrightarrow{k_{2,Q}} H_{n+1}Q^{n-1} + HCO_3^-, n = 0, 1 \tag{17}$$

A third pathway, the direct hydration of CO_2 with water, is also possible, but has a rate constant of $\approx 6.7{*}10^{-4}$ $(Ms)^{-1}$, many orders of magnitude lower than that of the reaction with OH^- ($k_{2,OH} \approx 8300$ $(Ms)^{-1}$).[6,50,52,54] As a result, we expected that this reaction will only become relevant when the pH at the start of the absorption process is less than 7 (*i.e.*, when the molarity of pure water, $\approx 55M$ water is 8 orders of magnitude greater than the concentration of OH^-), and preliminary analyses indicated that this is rare for the conditions studied. In the few instances when this did occur, very little CO_2 is captured due to the low pH, and the process time prediction became dominated by the penalty function, limiting the impact of these conditions on our analysis (Section 2.3).

Previous work had assumed both reaction rate constants were the same ($k_{2,OH} = k_{2,Q}$) due to the rapid protonation and deprotonation reactions in aqueous media,[17] leading to an approximation where the effective concentration of sorbent was assumed to be the sum of the concentrations of all proton acceptors, *i.e.*, hydroxide ions and all deprotonated reduced species. However, based on absorption studies with tertiary and sterically hindered amines, which catalyze CO_2 absorption by accepting a proton from water to produce a hydroxide ion sorbent, the rate constant of the termolecular (3-molecule) reaction is often lower than that of the hydroxide-CO_2 reaction.[55–57] Because the concentration of deprotonated reduced quinones can be much higher than that of hydroxide, neither reaction can be assumed to dominate for all conditions, requiring both rates to be included in our model. We therefore extended the Krevelen and Hoftijzer model to accommodate the two parallel reactions (CO_2 + OH^- and CO_2 + H_2O + deprotonated reduced species) by modifying the calculation of the Hatta number, which represents the unitless ratio of the reaction rate and mass transport

(Eq. 18), and that of the instantaneous enhancement factor, E_i, which is the limiting enhancement factor if mass transport is fast.

$$\mathrm{Ha} = \frac{\mathrm{Ha_{num}}}{\mathrm{Ha_{den}}} = \frac{\text{Reaction rate}}{\text{Mass transport rate}} \tag{18}$$

For a single reaction of gas species A and sorbent B with rate constant k and stoichiometric coefficients a and b, respectively, the numerator of the Hatta number, $\mathrm{Ha_{num}}$, is related to the rate law equation via the boundary layer thickness δ_L (Eq. 19 - 21):

$$\frac{d[\mathrm{A}]}{dt}|_{\mathrm{rxn}} = -ak[\mathrm{A}]^a[\mathrm{B}]^b \tag{19}$$

$$\delta_L = \frac{D_\mathrm{A}}{k_L} \tag{20}$$

$$\begin{aligned} \mathrm{Ha}^2_{\mathrm{num}} &= k[\mathrm{A}]^a[\mathrm{B}]^b\delta_L \\ &= k[\mathrm{A}]^a[\mathrm{B}]^b\frac{D_\mathrm{A}}{k_L} \end{aligned} \tag{21}$$

where k_L is the reactor mass transfer coefficient, related to the boundary layer thickness via the diffusion coefficient of A in the liquid phase, D_A.

$$\delta_L = \frac{D_\mathrm{A}}{k_L} \tag{22}$$

For two parallel reactions, the instantaneous reaction rate would be additive, producing:

$$\mathrm{Ha}^2_{\mathrm{num}} = (a_b k_b[\mathrm{A}]^{a_b}[\mathrm{B}]^b + a_c k_c[\mathrm{A}]^{a_c}[\mathrm{C}]^c)\frac{D_\mathrm{A}}{k_L} \tag{23}$$

where k_b is the rate constant of $a_bA + bB$ and k_c is the rate constant for $a_cA + cC$. The Hatta number denominator, $\mathrm{Ha_{den}}$, represents the physical absorption rate of A in the absence of reactions, depending only on the mass transfer coefficient and the concentration gradient, with the assumption that the gas phase concentration of A is much greater than that of the bulk solution.

$$\mathrm{Ha}_{\mathrm{den}}^2 = k_L[\mathrm{A}] \tag{24}$$

The ratio of these terms gives the unitless Hatta number for two parallel reactions (Eq. 25).

$$\mathrm{Ha} = \frac{\mathrm{Ha}_{\mathrm{num}}}{\mathrm{Ha}_{\mathrm{den}}} = \frac{\sqrt{D_{\mathrm{A}}(a_b k_b [\mathrm{A}]^{a_b-1}[\mathrm{B}]^b + a_c k_c [\mathrm{A}]^{a_c-1}[\mathrm{C}]^c)}}{k_L} \tag{25}$$

The instantaneous enhancement factor E_i for a single reaction is defined:

$$E_{i,1\mathrm{rxn}} = 1 + \frac{aD_{\mathrm{B}}[\mathrm{B}]}{bD_{\mathrm{A}}[\mathrm{A}]} \tag{26}$$

If multiple reactions occur in parallel, the effect on the enhancement factor should be similarly additive:

$$E_{i,2\mathrm{rxn}} = 1 + \frac{a_b D_{\mathrm{B}}[\mathrm{B}]}{b_b D_{\mathrm{A}}[\mathrm{A}]} + \frac{a_c D_{\mathrm{C}}[\mathrm{C}]}{c_c D_{\mathrm{A}}[\mathrm{A}]} \tag{27}$$

The diffusion coefficient of hydroxide was estimated as $D_{\mathrm{OH^-}} = 5.2{*}10^{-5}$ cm^2/s,[58] while the diffusion coefficient of the deprotonated hydroquinone in water was assumed to be the same as that of CO_2 in water ($\approx$ 5–20*10^{-6} cm^2/s)[6] based on diffusion coefficients of other small nucleophilic sorbents in water (2.85–5.75*10^{-6} cm^2/s);[59] we use the lower bound of the CO_2 diffusion coefficient as a conservative underestimate for our analysis. The rate constant for the reaction with hydroxide was assumed as $k_{2,\mathrm{OH}} = 8300$ $(\mathrm{Ms})^{-1}$.[6,50,52,54] The rate constant for the termolecular reaction with reduced hydroquinone has not been reported in the literature (17), and instead was manipulated as a variable of study, constrained by expected correlations between the rate constant and other chemical properties from other sorbents that capture CO_2 via a similar termolecular mechanism (Section 2.4).

For the combined absorber, the process must be rate limited by the current, not the mass transport. Because the CO_2 flux (Eq. 13) presents a physical limit that cannot be exceeded, there exists an upper bound for the current density above which the combined absorber is mass transport limited; above this value, the combined absorber would perform similarly

to the separated reactor configuration. To estimate that upper limit, we converted the flux to a current density ($j_{\max}$) using the ratio of coulombs passed after pretreatment, q_{abs}, to the moles of carbon captured (Eq. 28). For this calculation, we assumed that because the CO_2 flux model assumes a thin film of liquid, the electrolyte-electrode interface area should be similar to the vapor-liquid interface area. While at a first glance, this conversion would indicate that the current density and flux are interchangeable to give the same rate for the separated and combined absorbers, the combined absorber typically started absorption at a lower pH due to its less extreme state of charge, resulting in a smaller concentration gradient and estimated flux, J (Eq. 13).

$$j_{\max} = J \frac{q_{\text{abs}}}{\text{DIC}_{\text{anode}} - \text{DIC}_{\text{cathode}}} \tag{28}$$

To compare the CO_2 flux of the separated reactors to the maximum current density of the combined absorber, we divided the total moles of the corresponding reaction by the relevant rate (Eq. 29), *i.e.*, normalizing the flux by the moles of CO_2 exchanged and the current by the total coulombs passed. The resulting metric, t_{res}, estimated the amount of interfacial area needed per liquid flow rate. Given our assumption that the electrolyte-electrode and vapor-liquid interface areas should be of a similar magnitude, we frame this metric as the normalized liquid-phase residence time in the absorber (henceforth, normalized residence time) that accounts both for how quickly the reaction occurs and how much of that reaction can occur.

$$t_{\text{res}} = \begin{cases} \frac{\text{DIC}_{\text{anode}} - \text{DIC}_{\text{cathode}}}{J}, & \text{Separated unit operations} \\ \frac{q_{\text{abs}}}{j_{\max}}, & \text{Combined, Staged Current} \\ \frac{q_{\text{tot}}}{j_{\max}}, & \text{Combined, Constant Current} \end{cases} \tag{29}$$

When considering the amount of charge passed in the combined absorber configuration, the total charge in Eq. 29 can be taken as either the total charge passed during the entire

cathodic step (q_{tot}), or it can include only the charge after pretreatment (q_{abs}). While the former case would be a simpler design because it would require only one cathodic half-cell, it would increase the normalized residence time by operating the pretreatment process at low current densities. Consequently, we included both possibilities in this study to determine under what conditions it would be essential for the pretreatment process to be a separate electrochemical half-cell with a higher current density.

2.3 Penalty Functions

The range of chemistries that we simulated varied in the amount of the feed gas CO_2 they could capture, ranging from failing to capture any CO_2 to being able to capture >99.99% of CO_2 in the feed gas. Importantly, conditions that remove less CO_2 have lower thermodynamic limits for their work of separation, and their normalized residence time should decrease because fewer CO_2 molecules or electrons need to be transferred. Given our interest in low energy demand and low process time processes, we needed a method of distinguishing between conditions that achieve promising energy demands and process times with sufficient capture from those that achieve those goals as a result of limited CO_2 removal. We empirically tuned penalty functions (Figure S1) for both the energy demand and normalized residence time such that conditions capturing << 90% of the CO_2 from typical coal power plant flue gas ($P_{\text{min}} > 0.1P_{\text{feed}}$) would not interfere with our optimization of the energy demand and process time estimates (Section 2.5). We selected a 90% capture target due to the stated goals by the US Department of Energy for carbon capture technologies.[11] Recognizing the Department of Energy's caveat that technologies that capture less than 90% of the feed gas CO_2 may still be viable if their costs are sufficiently low, we used an exponential penalty function rather than the typical binary cutoff of other optimization studies,[60] designed and empirically tuned on a preliminary dataset such that conditions that captured $50 - 89\%$ of the CO_2 had a slight perturbation (Eq. 30). This more gradual form of the penalty function prioritizes conditions that capture > 90% of the CO_2, but does not explicitly exclude conditions that approach

but still fail to meet this target if the energy demands and process times are sufficiently low. The application of the penalty function to the energy demand and normalized residence time was adjusted to account for the different scales and resolutions needed for evaluating these two process performance metrics (Eq. 31-32).

$$\ln p = 0.489 \log_{10} P_{\text{min}} + 1.726 \tag{30}$$

$$W^*_{\text{cyc}} = W_{\text{cyc}} + p \tag{31}$$

$$t^*_{\text{res}} = t_{\text{res}}(5p + 1) \tag{32}$$

In these equations, P_{min} is the minimum CO_2 partial pressure achieved after reductive sorbent reactivation in the separated unit operation configuration (Figure 1bd) and W^*_{cyc} and t^*_{res} are the penalty-adjusted electrochemical work and normalized residence time, respectively. All data presented here of the energy demand and normalized residence time are the penalty-adjusted forms.

2.4 Process Variables of Study

The energy demand and capture rate of the carbon capture process were functions of solution chemistry and operating variables. For this study, we studied the combined effects of seven variables: the total quinone concentration ([Q]), the concentration of additional base ([NaOH]), the two pK_{a} values of the reduced hydroquinone, the rate constant of the termolecular carbon capture reaction, the state of charge midpoint, and the state of charge range. The first four variables have been previously investigated and were restricted to the same limits,[17] while we included the latter three variables due to this study's emphasis on the absorption rate. Like previous studies, we constrained this study to the solution chemistry and operating conditions that fit established chemical trends for substituted quinones because many variables are correlated (Table 1).

Table 1: Bounds and relationships for the seven variables of interest.

Variable	Lower Bound	Upper Bound	Source
pK_{a1}	2	13.5	17,61
pK_{a2}	pK_{a1}	pK_{a1} + 5.5	17,61
$\log_{10}$[Q]	-2	0.5	17,28
$\log_{10}$[NaOH]	$\log_{10}$[Q] - 7	$\log_{10}$[Q] + 0.7	17
$\log_{10} k_{2,Q}$	1.0885 pK_{a1} - 9.416	1.0885 pK_{a1} - 8.166	Figure S2
Median y_r	0.15	0.85	
Range y_r	0.1	0.95	

Existing studies with quinones for electrochemical CO_2 capture do not provide sufficient information to estimate rate constant $k_{2,Q}$.[28–30,32] Additionally, we could find no information on CO_2 absorption kinetics catalyzed by proton acceptors besides amines, CO_3^{2-}, and OH^-, so we assumed the rate constant for the termolecular reaction followed the same Brønsted relationship between $k_{2,Q}$ and pK_a as tertiary and sterically hindered amines, which enhance CO_2 absorption rates through a similar mechanism (Figure S2).[55,56] We expected that the rate constant for hydroquinones would be slightly slower than for amines due to steric hindrance, so we expected that this trend caused our normalized residence time predictions to be overestimates. As a result, we have high confidence in our conclusions of which conditions would fail to achieve the energy and process time design goals but lower confidence in assessing which conditions were better than others in minimizing the process time. For the purposes of sampling (Section 2.5), the variable of interest is the regression error between the rate constant and the Brønsted relationship, which fell between -0.75 and +0.5 for $> 95\%$ of the available dataset from the literature,[55,56,62–65] and we used the lower of the two pK_a values to partially compensate for the overestimation.

The midpoint and range of the state of charge were of interest because past work on this pH-swing system showed that the magnitude of the hysteresis between the anode and cathode potentials caused by CO_2 concentration differences may not be symmetric around a state of charge of 0.5.[17] As a result, changing the operating window for the state of charge, whether narrowing the range or offsetting it to more reducing or oxidizing conditions, may minimize

the hysteresis and therefore minimize the energy demand. Additionally, the total coulombs passed was directly proportional to the range of the state of charge, and thus increasing this variable increased the normalized residence time of the current-limited combined reactor. In order to avoid extreme states of charge, at which small state of charge perturbations rapidly change the electrode potential, we applied an additional restriction to the state of charge range that prevented the state of charge from being less than 0.025 or greater than 0.975 (Table 1).

2.5 Adaptive Sampling Methods

We used an adaptive sampling approach to minimize the size of the dataset necessary to make our conclusions with confidence. We used an adaptive sampling approach to minimize the size of the dataset necessary to make our conclusions with confidence. This experiment design involved developing "acquisition functions" that predicted how much new information a specific condition should provide if sampled next based on data that has already been collected and the research question of interest. By iteratively sampling the point that maximized the acquisition function and updating the function based on the new datum, the resulting dataset prioritizes samples in areas of interest and minimizes redundant samples to maximize the statistical utility of our dataset when answering our research questions (Section 2.6). Our initial dataset was sampled using five separate 10-point resolution Latin hypercube designs combined with 150 additional random samples from a multivariate uniform distribution. The 10 lowest energy demands and normalized residence times for each reactor configuration were used as starting populations for multiple independent coarse resolution single-objective optimizations via a genetic algorithm (10 generations of population 10).[66,67] The combined dataset of the original random samples and the estimated single-objective optima then informed Pareto front estimation using Gaussian processes (100 points per reactor configuration).[68] This Pareto front described the set of optima when considering both energy demand and process time, varying their relative importance in the optimization. A point is

part of the estimated Pareto front if no condition has been found with both a lower energy demand and a lower normalized residence time. Because both objective functions spanned multiple orders of magnitude and were strictly positive after applying the penalty function (Section 2.3), we used the log transform of both the energy and normalized residence time metric for our analysis. This transformation prevented a few extremely large energy demand or normalized residence time results from impacting the quality of the fit to the Gaussian process during adaptive sampling for the Pareto front. We estimated the single objective optima and Pareto fronts for each reactor configuration in parallel, then combined the datasets such that for any set of solution chemistry and operating conditions sampled, we knew its energy demand and normalized residence time in all three reactor configurations, allowing direct comparison of the impact of the combined absorber and the pretreatment step current density assumption.

We followed Pareto front estimation with multiple contour estimations using a previously established Gaussian process-based method.[17] Contour estimation prioritizes collecting data that would fall along a specific boundary, *e.g.*, input conditions with a specific energy demand value. By collecting more data close to that contour of interest, we could more accurately predict whether a yet-untested condition would fall above or below the boundary. In this multi-objective case, some contours of interest defined regions of both low energy and low rate, increasing confidence in predictions of whether an untested condition would meet both criteria simultaneously. Because we were interested in multiple contours defined by different criteria of interest (Table 2), we performed multiple contour estimation procedures in series from the least restrictive to the most restrictive. The contours of interest were defined as: (*1*) 1 log removal (90% capture) of CO_2, as determined by the minimum lean gas pressure, (*2*) conditions that were close to the Pareto front for the given reactor system, (*3*) being better than the temperature swing benchmark process as reported in the literature,[6–8,13,69] (*4*) being capable of meeting conservative carbon capture performance targets,[6,7,11,13,16,70,71] and (*5*) maximizing the benefit and minimizing the drawbacks of the combined absorber. For

contours (*2*)-(*4*), each reactor configuration had its own acquisition function, so the reactors were treated in parallel at each iteration to produce three new data points per iteration. Contours (*1*) and (*5*) were defined with a single acquisition function, and thus ran for three times the number of iterations to obtain the same number of adaptive samples ($n = 60$).

Table 2: Regions of interest that guided adaptive sampling for contour estimation.

Description	Targets	Source
(*1*) 1 log removal	$P_{\min} \leq (P_{\text{lean}} = 0.1 P_{\text{feed}})$	DoE Target[11]
(*2*) Near the Pareto front	$W_{\text{cyc}} \leq 1.2W'$ & $t_{\text{res}} \leq 1.2t'$	$(W_{\min}, t')$ and $(W', t_{\min})$ are the single objective minima
(*3*) vs. temperature-swing benchmark	$W_{\text{cyc}} \leq 48$ kJ$_e$/mol C & $t_{\text{res}} \leq 848$ sm^2/L	6–8,13,69
(*4*) vs. CO_2 capture performance targets	$W_{\text{cyc}} \leq 25.2$ kJ$_e$/mol C & $t_{\text{res}} \leq 72.2$ sm^2/L	6,7,11,13,16,70,71
(*5*) Maximized combined absorber benefit	$(W_{\text{cyc}}^{\text{sep}} - W_{\text{cyc}}^{\text{comb,staged}})/W_{\text{cyc}}^{\text{sep}} \geq 0.5$ & $(t_{\text{res}}^{\text{comb,staged}} - t_{\text{res}}^{\text{sep}})/t_{\text{res}}^{\text{sep}} \leq 0.5$	This study

We defined conditions as being close to the Pareto front if their energy demand and normalized residence time were less than those of the pseudo-nadir point, defined as (W', t') if the single-objective optima for the reactor were $(W_{\min}, t')$ and $(W', t_{\min})$, increased by 20%. We approximated the temperature swing process as requiring 120 kJ of thermal energy (kJ$_t$) per mol C,[7,69] which would be equivalent to approximately 48 kJ of electrical energy output (kJ$_e$) per mol C in a coal-fired power plant.[6,13] We estimated the requisite normalized residence time as 848 s m^2/L using data from Rabensteiner et al.[8] While it may be unfair to compare the normalized residence time of electrochemical CO_2 capture processes to that of the heat-based process due to anticipated cost savings from the reduction in the energy demand, an analysis to compare monetary cost is outside the scope of this analysis due to the geographic and temporal variability of the cost of energy and materials. Additionally, a direct comparison allows for the possible consideration of retrofits of existing heat-based systems without substantially changing the absorber. We therefore interpret this process time target as a benchmark for assessing feasibility based on what already exists rather than a definitive target to reach, which is necessary to contextualize our calculations given that

our process time estimates span multiple orders of magnitude. For the conservative target values, we used 25.2 kJ_e/mol C, based on the energy demand target set by the Department of Energy for carbon capture systems in electrical energy units using the same heat-to-electricity assumption[11,16,72] and adjusted for an idealized 70% electrochemical energy efficiency.[18,73] The normalized residence time for this criteria was determined based on the maximum estimated CO_2 flux[6] and the maximum CO_2 removal based on absorption isotherms of CO_2 in the industry standard of 30wt% MEA solution capturing at 40°C and releasing at 120°C.[7,70,71] We defined the maximum combined absorber benefit as a combined absorber that reduced the energy demand by at least 50% and increased the normalized residence time by no more than 50%; these values were based on simulation results up to that point.

2.6 Statistical Methods

Because an adaptive sampling procedure was used to collect the dataset, simple descriptive statistics of the dataset would propagate the adaptive sampling procedure's bias towards the Pareto front and the contours of interest. Additionally, with the many process variables of interest, it would be difficult to isolate the individual variable contributions from the dataset alone. Therefore, while some trends may be discernible directly from the adaptively sampled dataset, we used the data to train surrogate models that could then be described using more easily interpreted statistical and data visualization methods. We specifically leveraged the existing Gaussian process models from the adaptive sampling procedure to assess how likely a particular set of process variables would meet the coupled energy-residence criteria defined by the contours of interest (Table 2). We specifically calculated partial dependence plots for each variable to assess its impact on the probability of falling inside the regions of interest defined by each selection criterion (Table 2).[17,74,75] Partial dependence plots simplify complex multivariate functions to the average behavior when a single variable is known and all others are taken from a random distribution. By changing the value of that single known variable, the impact of that single variable on the output function can be visualized,

with the aggregate impact of the other variables represented in the confidence interval. A partial dependence plot for each process variable under study was estimated using a 50-point resolution for that single known variable, with each point representing the median estimated by Monte Carlo sampling of possible chemical inputs ($n = 1000$). Based on prior work,[17] for this analysis, we used the solution chemistry variables in the form most likely to be measured and reported and not the transformed and decorrelated variables as they were defined during adaptive sampling. While this meant that strongly correlated variables gave nearly identical partial dependence plots and limited our mechanistic explanations because correlated variables could not be decoupled, this practice limited potential biases that emerge from transforming variables and enhanced interpretability and decision-making utility by referring to measurable properties. We suggested ranges for each variable based on the conditions that achieved at least half of the maximum probability in the partial dependence plot. Partial dependence plots were also used to inform variable importance rankings for meeting the selection criteria defined by each contour (Table 2).[17] These importance rankings qualitatively suggest which properties should be prioritized in the event trade-offs must occur when translating this purely computational work to physical reality.

We additionally created random forest models that connected the variables of interest to the minimum lean gas CO_2 partial pressure, the maximum amount of CO_2 captured per cycle, the minimum energy demand, and the minimum normalized residence time.[76] Although the Gaussian process surrogate models accurately predicted the categorical outcome of if a point met the criteria defined by the contours of interest (Table 2), they were less accurate at predicting quantitative output values. We selected random forest models over other regression models due to their flexibility and tunability when fit to high-dimensional datasets, allowing us to balance fitting the data well and overfitting. We note that while the fit quality of these random forest models worsened as the energy demand and normalized residence time estimates were much higher than the values of the contours of interest due to sparse sample resolution in those regions (Figure S3), the random forest model trends provided some insight

into why certain probabilities were high or low.

3 Results & Discussion

3.1 Impact of the Combined Absorber

The adaptively sampled dataset shows a clear difference among the three reactor configurations (the separated unit operations baseline, the combined absorber with a constant current density, and the combined absorber with a staged current density) in terms of their minimum energy and normalized residence time requirements (Figure 2). Note this figure omits many of the $n = 823$ adaptively sampled conditions to maintain resolution on the low energy-low process time region of interest (full dataset in Figure S4). As expected from the literature,[14,15] both combined absorber configurations produced lower energy demands, bringing the minimum energy of electrochemical carbon capture close to the minimum thermodynamic work of separation, $W_{\text{sep,min}} \approx 5.9$ kJ/mol for 90% capture from a 0.15 atm feed gas, although consistent with past modeling work,[14,15,17] the minimum energy demands could be much greater than this physical limit.

The minimum energy demand for electrochemical carbon capture was generally low compared to both the present-day temperature swing benchmark and the DoE carbon capture targets regardless of the reactor configuration. Having a minimum energy lower than the carbon capture target was particularly noteworthy, as the target energy demand was corrected to assume reasonable industrial-scale inefficiencies of electrochemical systems.[18,73] In total, approximately 38% of solution chemistry and operating conditions within the bounds set by this study would meet the energy demand target using separated unit operations, increasing to 43% using a combined absorber (Table 3). Note that this fraction is lower than the fraction of data points meeting the criteria ($\approx \frac{2}{3}$ of the dataset for all conditions) because the adaptively sampling procedure biased the dataset towards low energy-low residence time conditions.

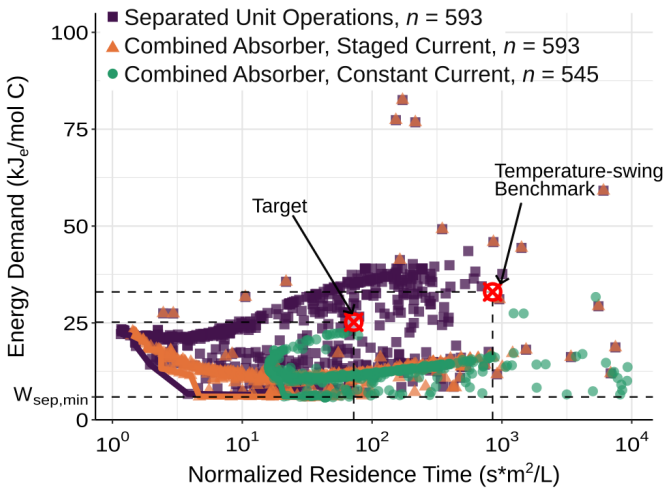

Figure 2: The adaptively sampled minimum electrochemical energy demand and normalized liquid-phase residence time in the absorber for the three configurations of study. Red ⊗ symbols denote the points that define the contours of interest (*3*) and (*4*). $W_{\text{sep,min}}$ is the minimum thermodynamic work of separation for 90% capture from a 15v% CO_2 feed gas. Note: The figure is restricted to the low energy-low residence time conditions; full dataset ($n = 823$) in Figure S4.

Unlike prior work that simulated PCET-driven carbon capture that also used the separated unit operation configuration,[17] we found greater difficulty in meeting the process rate metric, with only 47% of conditions improving upon the temperature swing benchmark compared to approximately 65% in the previous study. We attributed this to considering the normalized residence time in this study, while the previous study only considered the maximum CO_2 flux. This disparity arose from the fact that increases in the flux were often

Table 3: Probability of a randomly-sampled solution chemistry meeting specified criteria ($n = 3000$).

		Separated Unit Operations	Combined Absorber, Staged Current	Combined Absorber, Constant Current
vs. MEA	$W_{\text{cyc}} < W_{\text{MEA}}$	0.44	0.48	0.48
	$t < t_{\text{MEA}}$	0.47	0.46	0.30
	$W_{\text{cyc}} < W_{\text{MEA}}$ & $t < t_{\text{MEA}}$	0.36	0.39	0.27
vs. Target	$W_{\text{cyc}} < W_{\text{target}}$	0.38	0.43	0.43
	$t < t_{\text{target}}$	0.28	0.26	0.17
	$W_{\text{cyc}} < W_{\text{target}}$ & $t < t_{\text{target}}$	0.20	0.22	0.15

accompanied by increases in the carbon capture capacity, and thus the benefit in the CO_2 flux would be counteracted by the increase in total mass exchanged. We note that our "minimum" normalized residence time is the interfacial area-adjusted residence time required for $> 99\%$ of the maximum sorbent usage, and thus could be reduced should a lower ΔDIC be sufficient for design goals. However, a 2-fold decrease in the residence time, equivalent to only using half of the carbon capture capacity, only increases this probability from 47% to 50%. For the probability estimate from this study to be similar to that of the previous study, systems can only use approximately 10% of their full carbon capture capacity.

The combined absorbers generally required greater normalized residence times because the electrochemical reaction must be slower than CO_2 mass transport, leading to lower probabilities of meeting either process time criteria (Table 3). This led to a greater than 10-fold increase to the normalized residence time requirements for the combined absorber with a constant current density, lowering the likelihood of meeting any design target that considered the process time. Staging the current such that the pretreatment step's time contribution could be considered negligible compensated for most, but not all, of the process time increase, indicating that the decrease in the carbonic acid concentration gradient due to incomplete sorbent reactivation had a small but potentially measurable impact on the CO_2 flux. Combined with the reduction in the energy demand, this minimal change to the normalized residence time for the combined absorber with staged current led to slightly higher probabilities of meeting the energy demand and process time targets simultaneously.

Interestingly, the Pareto front for the combined absorber configuration with staged current was nearly identical to that of the baseline of separated unit operations (Figure 2). This indicated that for conditions that were nearly Pareto-optimal when the electrochemical half-cell and absorber were separate unit operations, the benefit of combining the two reactors was minimal, as was the penalty to the normalized residence time. To identify why these conditions showed little difference in both energy demand and normalized residence time regardless of the reactor configuration, we used the adaptively sampled dataset (Figure

2) to calculate the change in these two objective functions as a result of changing only the reactor configuration (Figure 3). Each data point represents the percent change in the idealized energy demand and normalized residence time if the 4-stage separated unit operations condition was changed to a combined absorber configuration with the same process variable conditions (Table 1). Given that the thermodynamic process models of the combined absorber configurations only differ from those of the separated unit operation configuration when the partial pressure of CO_2 is less than that of the lean gas target (set at 1 log removal = 90% capture), conditions that fail to meet the 90% capture target would have similar species concentration profiles for all reactor configurations. It follows, then, that the greatest differences between the two combined and separated configurations would occur when the concentration profile differences are greatest, occurring when the removal capacity of the separated unit operation configuration, presented in log units (Eq. 33), increased.

$$\text{Removal capacity} = \log_{10}(P_{\text{feed}}/P_{\text{min}}) \tag{33}$$

Consistent with this hypothesis, for the combined absorber with staged current, conditions that showed the smallest energy demand and normalized residence time differences between the separated and combined configurations occurred when the maximum CO_2 removal capacity was lowest. As the maximum CO_2 removal capacity increased, the combined absorber configuration led to a greater decrease in the energy demand (median 23%, up to 67%) and a greater increase in the normalized residence time (median 19%, up to 290%). Both trends are expected because the combined absorber has a lower extent of separation, decreasing the energy demand, but also a smaller concentration gradient, decreasing the maximum rate. Our results differ from the existing literature that estimated that the combined absorber would lead to an approximately 40% reduction in the energy demand for most calculated conditions,[15] although our wider range of surveyed solution chemistries explains this difference. Notably, the Pareto fronts for all conditions generally occur when achieving as close to 1 log removal as possible (Figure S5), which, combined with these results, explains

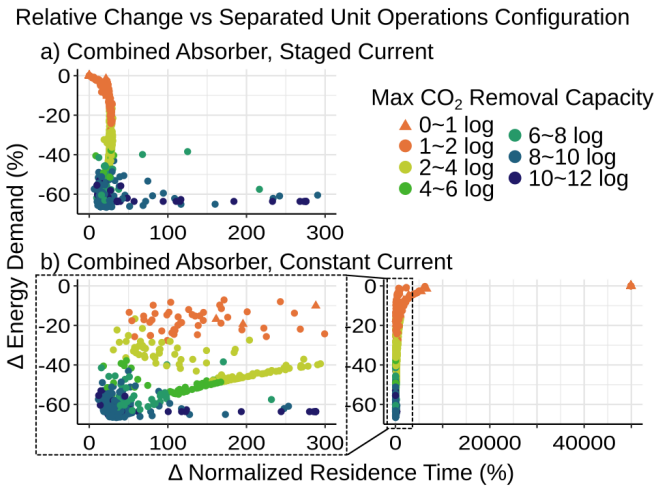

Figure 3: Relative change in the energy demand and normalized liquid residence time caused by changing the separated unit operation configuration to the combined absorber configuration assuming (a) staged current or (b) or constant current, with (inset) a zoom in on the constant current assumption data to have the same x-axis as the staged current assumption for direct comparison. Color is the maximum possible CO_2 removal capacity in the separate unit operation configuration; the combined process is limited to a maximum of ≤ 1 log removal.

why the Pareto fronts for the separated and combined absorber with staged current were similar.

Unexpectedly, for the combined absorber operated with constant current, maximizing the reduction in the energy demand also minimized the penalty to the normalized residence time. Initially it was believed that this trend was purely due to the scale of the x-axis, as the residence time increases much more when changing from the separated configuration to this combined configuration, but even when narrowing the scope to the same regime as the staged current configuration (Figure 3b), the inverted trend is still observed. Given that the only difference in normalized residence time between the staged and constant current configurations was the inclusion of a pretreatment charging step in the process time estimate, this difference suggested that solution chemistry conditions with lower removal capacities were more impacted by the pretreatment charging time. This was reflected in the energy-residence time relationships (Figure S5), which showed that conditions with high maximum

removal capacity ($>$ 6 log removal) were nearly identical for the two combined absorbers, but conditions with lower removal capacity had substantially higher normalized residence times upon adding the pretreatment charging time. As a result, unlike for the other two configurations studied here, the low normalized residence time portion of the Pareto front for the combined absorber with constant current included conditions with moderate maximum removal capacities (2-6 log removal).

To discern why the pretreatment charging time became more significant as the maximum removal capacity decreased for the constant current condition, we reanalyzed the adaptively sampled dataset with the aim of identifying if there was a third variable that could connect the pretreatment charging time to the maximum removal capacity S1.1. First, we found that the total number of Coulombs required to reach 90% removal was generally consistent, particularly when $>$99% of the CO_2 could be captured (Figure S6a). However, the total number of Coulombs passed generally increased with increasing removal capacity, and thus the percentage of the current, and consequently the process time, dedicated to pretreatment was generally higher at low removal capacity (Figure S6b), leading to a large difference in the process time at low removal capacities (Figure S6c). This difference was exacerbated by the fact that the current density at which the system would transition from electrochemically rate limited to CO_2 absorption rate limited, while spanning multiple orders of magnitude, never exceed $\approx$ 5 mA/cm^2, with lower transition current densities tending often occurring alongside lower removal capacities and less CO_2 captured per cycle (Figure S7ab). This upper bound of $\approx$ 5 mA/cm^2 occurred because the enhancement factor, E, is upper bounded by the enhancement for an instantaneous reaction, E_i, in turn bounding the CO_2 absorption rate that this current density cannot exceed. While this upper limit current is similar to bench-scale experimental current densities employed by electrochemical carbon capture,[28,32,35,77] it is lower than the expected 10-100 mA/cm^2 that has been proposed to be required at industrial scales[25] and lower than many electrochemical pH-swing based carbon capture processes (Table S1). We additionally note that redox flow batteries using aqueous quinones,

on which the electrochemical cell for this system is often based,[14] operate at current densities up to 50-100 mA/cm^2,[78] indicating that these higher current densities are possible without prohibitive resistive losses.

Collectively, these results corroborate past analyses that suggest that combining the cathodic sorbent reactivation step with CO_2 absorption would lead to lower energy demands, but provide the additional caveat that doing so will likely make the process prohibitively slow. It is possible for the absorption process time to decrease to near parity with the separated reactor configuration by pretreating the solution at high current densities until the target lean gas partial pressure, but we note that this analysis only calculated the lower-bound normalized residence time of the combined absorber configurations when the electrochemical and mass transport rates were equal to each other. In reality, the energy benefit of combining electrochemical sorbent reactivation with CO_2 absorption would only be observed if CO_2 mass transport across the vapor-liquid interface can be assumed to be instantaneous relative to the electron transfer reaction at the electrode, and thus the absorption process time of the combined absorbers should be much greater than those reported here.

Importantly, combining electrochemical reactivation with CO_2 absorption was often unnecessary for the electrochemical pH swing systems modeled in this study. Nearly one-third of randomly selected solution chemistry and operation conditions could be better than the temperature swing benchmark, and one-fifth would be able to meet the DoE design targets without combining these processes. Those probabilities only increased by a maximum of 3 percentage points upon combining the two reactors, if not decreasing due to the process time increase from slow pretreatment (Table 3). Additionally, as the solution chemistry conditions in the configuration with separated unit operations approached the Pareto front, the benefit of combining the reactors diminished (Figure 2). As a result, combining the absorber would only be necessary for solution chemistry conditions that consume too much energy, but it provides little benefit to conditions that already achieve low energy demands.

3.2 Individual Variable Effects on Energy Demand and Process Time

Given the relatively small fraction of potential solution chemistries and operating conditions that can meet the energy demand and process time targets under idealized conditions (Table 3), we used the adaptively sampled dataset to determine what specific conditions have the greatest likelihood of achieving low energy demands and low process times. We specifically trained surrogate models on the adaptively sampled dataset to minimize the impact of the bias introduced by the adaptive sampling procedure when relating the process variables of interest to system-level outcomes like the maximum amount of CO_2 captured per capture cycle and the energy demand. We then used partial dependence plots to isolate individual variable contributions for ease of interpretation.[74,75] A preliminary analysis with random forest models as the surrogate models followed expected behavior: higher concentrations of sorbent and base, more basic pK_a values, and wider state of charge ranges generally led to both more CO_2 captured per cycle and lower minimum lean gas pressures (Figure 4ab). The concentrations had the largest impact on the amount of CO_2 captured per cycle, which was expected given that the amount of CO_2 captured is limited stoichiometrically by the amount of sorbent in solution. Conversely, the minimum lean gas pressure was most strongly impacted by the pK_a values, and indirectly the rate constant due to its assumed Brønsted relationship, because these pK_a values determine the pH after cathodic sorbent reactivation and therefore the percentage of inorganic carbon as carbonic acid.

Consistent with other models of the electrochemical pH-swing system,[17] we observed a diminishing return with the higher of the two pK_a values, where the difference between a highly basic and moderately basic redox molecule was negligible. Similarly, we observed that the concentration of additional base can be too high, shifting the pH window of operation outside of the buffer regime of the reduced redox molecule, limiting the change in the DIC throughout the process cycle.

Of note, these partial dependence plots indicate that knowing only one variable precisely

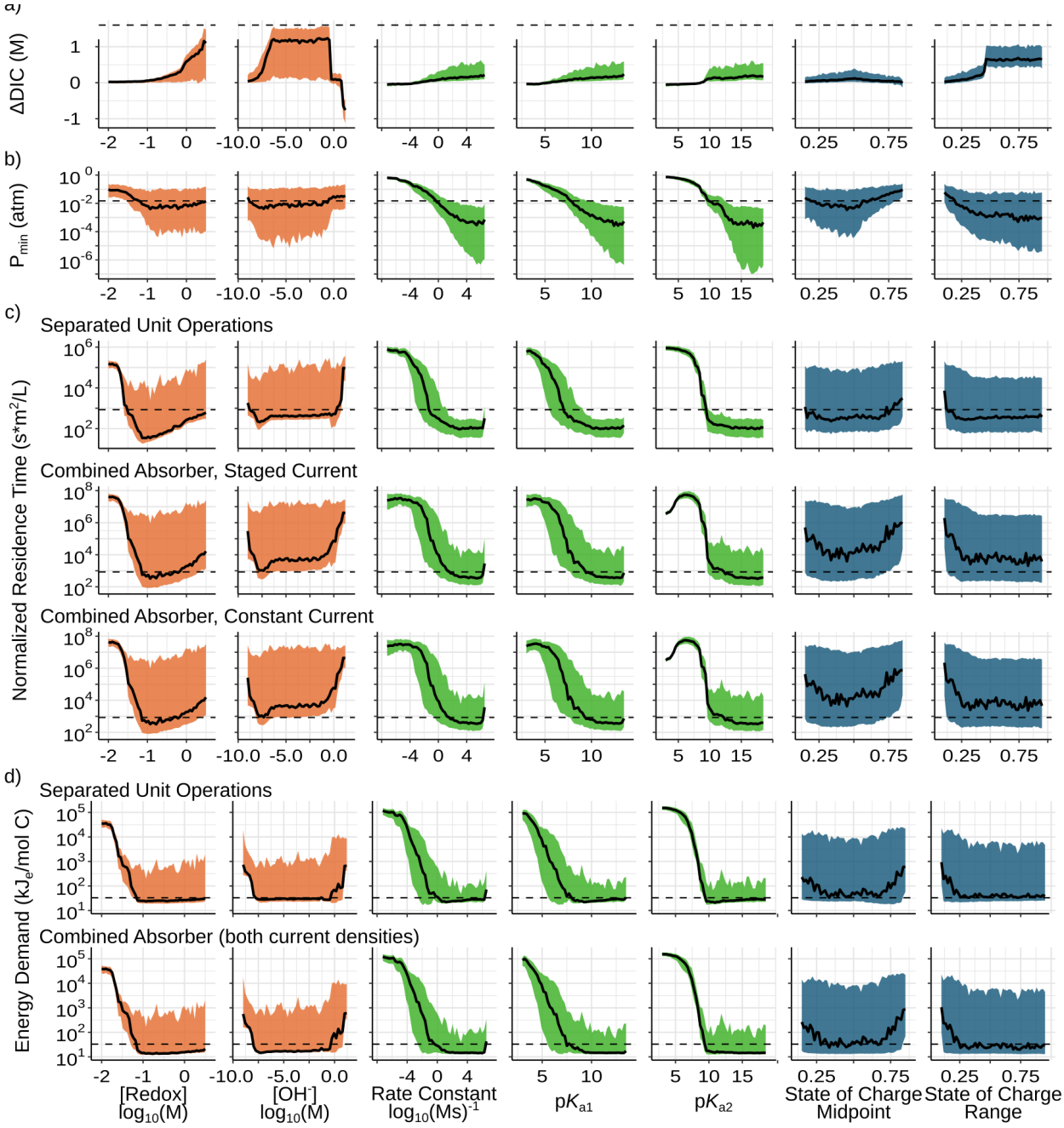

Figure 4: Partial dependence plots of: (a) the maximum amount of CO_2 removed, (b) the minimum lean gas CO_2 partial pressure, and (c) the normalized residence time of the three reactor configurations of study, and (d) the minimum energy demand for the separated and combined reactor configurations. Lines represent the median, colored bands are the interquartile range. Horizontal dotted lines are estimates for the temperature swing benchmark assuming 1 log removal. Colors indicate the variable type: concentration (orange, left 2), chemical property (green, middle 3), and operating condition (blue, right 2).

was not able to achieve the same amount of CO_2 removed per cycle as the temperature swing benchmark within its interquartile range (Figure 4a), suggesting that multivariate optimization would be necessary to achieve that goal. That is, optimizing only the pK_{a2} or the redox molecule concentration, for instance, cannot guarantee a process that captures as much CO_2 as the existing technology, and meeting this goal is only possible if multiple variables are tuned simultaneously. In contrast, the median minimum CO_2 partial pressure for most variables' partial dependence plots intersect the 90% capture mark, indicating that this goal would be relatively easy to achieve, but greater than 99% capture (2 log removal) would not be likely without intentional optimization of the state of charge range and chemical properties (Figure 4b). Contextualized with the relationship between the minimum lean gas CO_2 partial pressure and the magnitude of the energy benefits of the combined absorber (Figure 3), it follows that for a substantial fraction of solution chemistries and operation conditions, a combined absorber should have little impact on the minimum energy demand because most conditions do not have high enough CO_2 removal capacities for the combined absorber to have much impact.

To assess this point specifically, we estimated similar partial dependence plots for the energy demand. While conditions with high energy demands ($> 10^3$) were likely to be overestimated from these random forest models due to a low density of samples in those regions (Figure S3b), most energy demand predictions were below this value (Figure 4d). The shape of the partial dependence plots for the concentration and chemical properties were consistent with expectations based on past literature,[17] with similar optimal values for minimizing the energy demand. Greater state of charge ranges decreased energy demands, caused by the faster increase in the amount of CO_2 captured per cycle compared to the increase in energy demand per cycle. As a consequence, the midpoint of the state of charge achieved lowest energy demands at values close to 0.5, as this allowed the greatest state of charge range (Figure 4d). Interestingly, the midpoint slightly favored lower values, *i.e.*, more oxidized conditions. We believe that this is caused by complications of having too much

of the reduced species during the CO_2 release stage, because the moderately basic reduced species would increase the pH and limit the amount of CO_2 released.

The partial dependence plots for the normalized residence time (Figure 4c) are generally consistent with those of the energy demand (Figure 4d), suggesting that optimizing for energy would often optimize for the normalized residence time as well. The primary difference in the partial dependence plots between these two evaluation metrics was in their relationship with the concentrations: higher concentrations of both the redox molecule and additional base led to substantial increases in the median normalized residence time. In many cases, the minimum normalized residence time occurred at a redox molecule concentration similar to the minimum concentration necessary for energy demands below that of the temperature swing benchmark. We suspect this to be because at greater concentrations, the amount of either CO_2 captured or Coulombs transferred can increase faster than the corresponding rate if the other chemical properties were not properly optimized.

We highlight the difficulty in optimizing for both process time and energy demand simultaneously by presenting the partial dependence plots for the probabilities of meeting both the energy demand and normalized residence time criteria, estimated using Gaussian processes rather than random forest models due to their inherent inclusion of surrogate model uncertainty in this probability estimate (Figure 5). With the exception of the peak at the optimal redox molecule concentrations, the probabilities were generally low, rarely exceeding 25%, which was expected given the wide parameter space and results from other models of this system.[17] These probabilities decreased as the target values for the energy demand and normalized residence time decreased, *i.e.*, moving from region of interest (2) to (4) in Table 2. Consistent with our probability estimates from the full parameter space (Table 3), the combined absorber with staged current was slightly more likely to meet the selection criteria than the separated unit operations configuration due to its lower energies and small increase in the normalized residence time, although the difference was small after accounting for uncertainties in these probability estimates (Figures S8-S10).

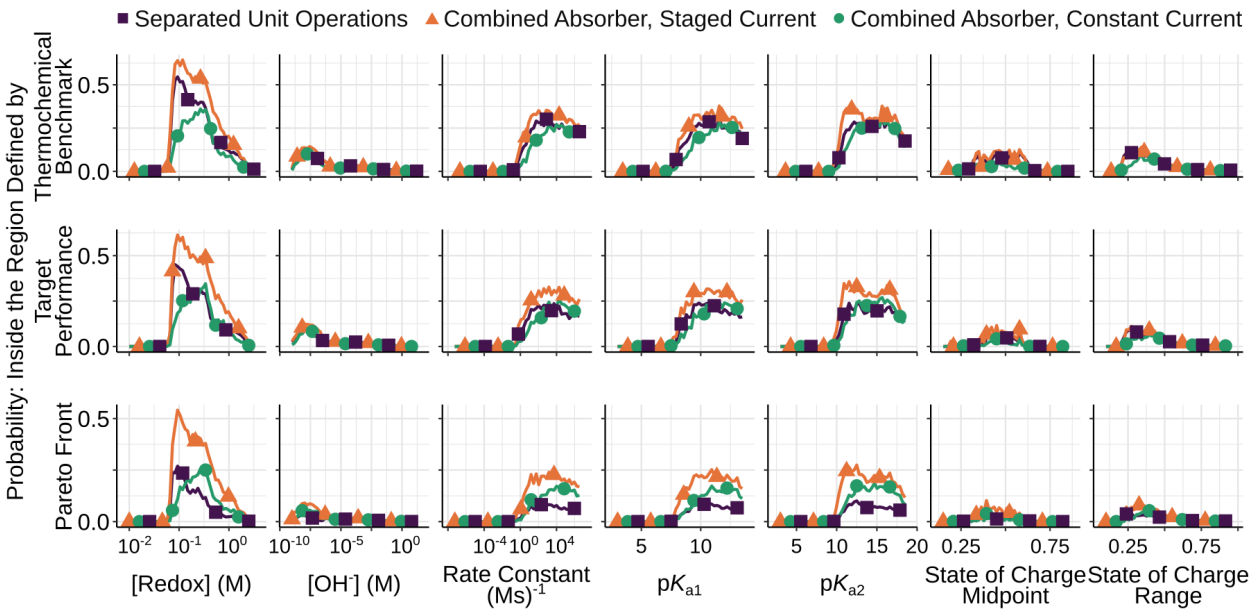

Figure 5: Mean probabilities of meeting both the energy and process time selection criteria defined by the coupled energy-process time regions of interest (Table 2), if only one variable is known, separated by reactor configuration (colors, symbols). Symbols are a subset of the data for visualization only.

With the exception of the concentration of additional base, the combined absorber with constant current required higher values for all input variables compared to the other two configurations. The optimal pK_a value was often multiple pH units higher, particularly as the selection criteria became more restrictive, and the peak in the redox molecule concentration was 2- to 3-fold higher (Figure 6). We believe the higher optimal pK_a values were due to their correlation with the reaction rate constant, leading to greater CO_2 fluxes and correspondingly greater maximum current densities, helping compensate for the amount of charge passed during pretreatment. While this is true for all conditions, the energy demand of all configurations decreases up to a p$K_{a,2}$ value of approximately 10, after which it increases slightly (Figure 4d), creating an energy demand-process time trade-off. Therefore, while the pK_a-rate constant correlation is true regardless of reactor configuration, very high rate constants are only necessary to achieve the process time targets in the combined configuration with constant current because the absorption rate becomes more important when it also af-

fects the pretreatment time. For the other configurations, the ease by which the process time criterion was achieved meant the detriment to the energy demand was substantial enough to shift the optimal pK_{a2} to slightly lower values. While the increase in the peak redox molecule concentration for the constant current configuration was unexpected given that this would increase the normalized residence time by increasing the total Coulombs transferred (Figure 4c), an increase in the total number of Coulombs transferred would reduce the fraction of the total charge associated with pretreatment, making the two combined absorber configurations more similar. In other words, the suggested redox molecule concentrations for the combined absorber with constant current were high because lower concentrations were substantially worse at achieving fast, low energy carbon capture, not because high concentrations became notably better with this reactor configuration. This was reflected in the upper bound of the suggested concentration range for the combined absorber with constant current, which was always less than or equal to that of the staged current configuration, and only the lower bound of this suggested range changed (Figure 6).

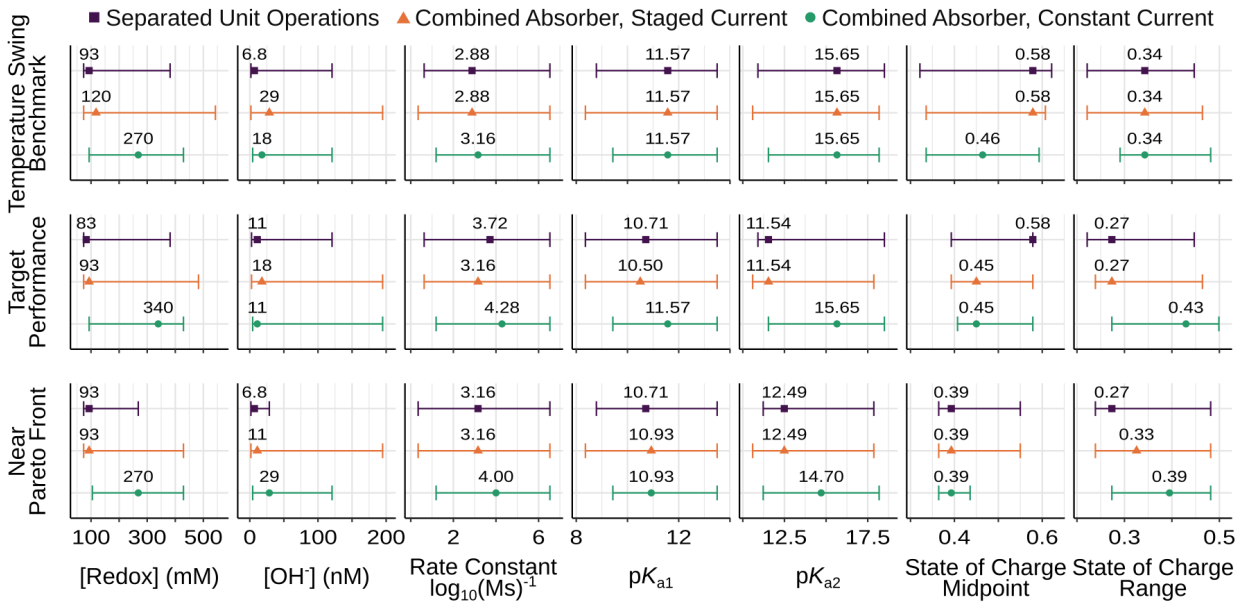

Figure 6: Suggested solution chemistry property domain for meeting the specified targets, defined as having at least half of the probability of meeting the target as the peak value (labeled point).

While these suggested variable ranges are useful in the abstract, in reality, one would be selecting a chemical compound for the process, not a set of independent properties, and thus the optimal concentration and pK_a values may not be achievable simultaneously. We therefore used the partial dependence plots for the probabilities (Figure 5) to infer which variables are most important for achieving each of the coupled energy-process time targets for each configuration (Section S1.2). Generally, the concentration of the redox molecule was the important variable to consider, followed by the higher of the two pK_a values (Figure S11). When making the energy and process rate target more restrictive, the concentration of the redox molecule became more important regardless of reactor configuration. In contrast, the lower process times caused by the combined reactor configurations, particularly that with constant current, led to an increase in the importance of the more basic pK_a value, although it only ever became more important than the redox molecule concentration with the constant current configuration when seeking to be better than the temperature swing benchmark. The importance of these two variables is consistent with perceived limitations from the literature, which report that this process is often limited by the redox molecule's solubility[28] and can be hampered by poor pK_a values.[14] However, we note that our suggested redox molecule concentrations (Figure 6), while higher than many of the reported experimental values (Table S1), are not as high as that used in the temperature-swing process (30wt% MEA $\approx$ 5 M) nor as high as others believed would be necessary for this process to be industrially viable.[14,28,29] Similarly, previous experimental reports believed the more basic pK_a value should be 13 at minimum,[14] whereas we found that the pK_a value that gave the greatest probability of meeting the design targets could be as low as 11 (Figure 6), *i.e.*, two orders of magnitude less basic, which is perfectly achievable with simple substitutions on 1,4-benzoquinone (Figure S12).

3.3 Implications for Electrochemical CO_2 Capture Process Design

While we found that the energy benefit of the combined absorber was often small compared to the increase in normalized residence time, there were conditions that showed a >50% decrease in energy demand and a <50% increase in normalized residence time regardless of current density assumptions (Figure 3a). We sought to determine what solution composition and operating conditions would fall in this regime of large energy benefit and low process time impact and consequently maximize the cost benefit of the combined absorber in order to inform when a combined absorber should be considered over improving the solution chemistry or operating conditions (Section S1.3). Partial dependence plots for the probability of falling within this regime indicated that this phenomenon was rare, with probabilities <0.1% for all variables except the state of charge range (Figure S13). This low probability was consistent with our finding that these conditions only occurred when the minimum CO_2 partial pressure would be less than 10^{-8} (Figure 3a), and the lower bound of the interquartile range of our estimates of the minimum lean gas CO_2 pressure rarely fell below 10^{-6} (Figure 4b). High state of charge ranges were the defining feature for meeting this selection criteria, after which the amount of base became the most important, which was similar to optimizing for the minimum lean gas CO_2 partial pressure (Figure S14). We note, however, that the values of the state of charge range and additional base concentrations that produced the largest energy benefits of the combined absorber configuration (Figure S13) were also those that are the least likely to achieve low energy, low process time carbon capture whether the two processes are combined or separate (Figure 5). Therefore, the energy demand benefit from combining the absorber and cathodic half-cell is likely to be small to moderate (0-40%) with a substantial increase in the absorption process time (Figure 3), particularly if the current density is set low enough that the electrochemical reaction would be instantaneous relative to CO_2 absorption instead of at parity like in this study.

Rather than designing a reactor that can perform electrochemical sorbent reactivation simultaneously with CO_2 absorption, optimizing the solution chemistry through proper re-

dox molecule selection is more likely to achieve industrially-viable electrochemical pH-swing carbon capture driven by PCET reactions. While a combined absorber can reduce the energy demands, most solution chemistry compositions do not decrease the partial pressure of CO_2 low enough for there to be a substantial energy demand benefit. The energy benefit will be even smaller if the electrochemical half-cell operates at current densities on par with modern industrial electrochemical operations,[78–81] which are greater than or comparable to the current density at which mass transfer and the electrochemical reaction have similar rates (Figure S7). In contrast, solution chemistry and operating condition variables have the potential to change the minimum energy demand by multiple orders of magnitude (Figure 4d), and many of the conditions that minimize the energy demand can also lower the normalized residence time (Figure 4c), unlike the combined absorber, which imposes an unavoidable trade-off (Figure 3).

We acknowledge, however, that this conclusion is limited by assumptions within our study design, most notably those related to our metric for the process time. While the CO_2 flux used in this study is a widely-used rate metric,[6,17,42–51] that metric does not account for how much of the reaction must occur, a key factor needed to be able to compare mass transfer-limited systems to current density-limited systems. We assumed that the CO_2 flux would be constant at the average value predicted by the absorber model until the system reached equilibrium with the inlet. In reality, the flux should decrease as the concentration gradient decreases closer to the gas inlet/liquid outlet at the bottom of the countercurrent exchanger. Not only did this underestimate the minimum normalized liquid residence time in the absorber by overestimating the flux near the end of the absorption process, but it also led to an inaccurate process cycle, which assumed a constant DIC increase and constant current density in the combined absorber. While we tried to compensate for the underestimation of the normalized residence time by comparing our values to each other and to the theoretical value obtained when using the same assumptions for the temperature swing benchmark, the magnitude of the impact of the inaccurate process cycle on both energy and process time could vary

among different solution chemistry and operating parameters. To properly account for this impact, one would need to model the gas and liquid phases throughout the absorber height explicitly, which was outside of the scope of this study due to its introduction of absorber geometry and packing material parameters as additional variables of study. However, we anticipate that correcting the process cycle of the combined absorber configurations would amplify the difference between the separated and combined absorbers given this study's intentional conservative underestimation of the combined absorber configuration's process time. Similar expanded models and experimental measurements are necessary to overcome limitations related to the energy demand, such as the variability of the current efficiency with current density and redox molecule diffusivities.

An explicit, spatially-resolved model of combined CO_2 transport across the vapor-liquid interface and electrochemical reactions would be better suited to exploring the effects of an anodic CO_2 desorber. Not only is a combined desorber more feasible at high current densities due to faster CO_2 desorption than absorption kinetics,[26,82,83] it could also control CO_2 bubble formation, reducing resistive losses and correcting a known issue limiting electrochemical carbon capture flow cell designs.[22,84] Importantly, a combined desorber should not require the pretreatment step because the gas phase in the desorber is either pure CO_2 or a combination of CO_2 and an easily condensable carrier gas. As a result, any absorption of CO_2 prior to sufficient electrochemical sorbent inactivation would not substantially affect the purity of the product gas in the way that it would affect the lean gas product from a combined absorber. While this work indicated that the 2-stage electrochemical carbon capture process is unlikely to be industrially viable due to the impact the combined absorber has on the process time, the 3-stage process with only a combined desorber may be a more appropriate avenue for reducing the minimum energy demand and increasing the energy efficiency with a limited impact on process time.

References

(1) Hoegh-Guldberg, O. et al. In *Impacts of 1.5°C global warming on natural and human systems*; Masson-Delmotte, V. et al. , Eds.; International Panel on Climate Change, 2018

.

(2) Stocker, T., Qin, D., Plattner, G.-K., Tignor, M., Allen, S., Boschung, J., Nauels, A., Xia, Y., Bex, V., Midgley, P., Eds. *Climate Change: The Physical Science Basis. Contribution of Working Group I to the Fifth Assessment Report of the IPCC*; International Panel on Climate Change, 2013

.

(3) Kriegler, E.; Luderer, G.; Bauer, N.; Baumstark, L.; Fujimori, S.; Popp, A.; Rogelj, J.; Strefer, J.; Vuuren, D. P. V. Pathways limiting warming to 1.5°C: A tale of turning around in no time? *Philosophical Transactions of the Royal Society A: Mathematical, Physical and Engineering Sciences* **2018**, *376*, 20160457

.

(4) National Academies of Sciences Engineering and Medicine, *Negative Emissions Technologies and Reliable Sequestration*; National Academies Press, 2019

.

(5) Keith, D. W.; Holmes, G.; Angelo, D. S.; Heidel, K. A Process for Capturing CO_2 from the Atmosphere. *Joule* **2018**, *2*, 1573–1594

.

(6) Wilcox, J. *Carbon capture*; Springer New York, 2012; pp 53–114

.

(7) Tobiesen, F. A.; Svendsen, H. F.; Hoff, K. A. Desorber Energy Consumption Amine Based Absorption Plants. *International Journal of Green Energy* **2005**, *2*, 201–215

.

(8) Rabensteiner, M.; Kinger, G.; Koller, M.; Gronald, G.; Hochenauer, C. Pilot plant study of ethylenediamine as a solvent for post combustion carbon dioxide capture and comparison to monoethanolamine. *International Journal of Greenhouse Gas Control* **2014**, *27*, 1–14

.

(9) Zhao, M.; Minett, A. I.; Harris, A. T. A review of techno-economic models for the retrofitting of conventional pulverised-coal power plants for post-combustion capture (PCC) of CO_2. *Energy and Environmental Science* **2013**, *6*, 25–40

.

(10) Markewitz, P.; Kuckshinrichs, W.; Leitner, W.; Linssen, J.; Zapp, P.; Bongartz, R.; Schreiber, A.; Müller, T. E. Worldwide innovations in the development of carbon capture technologies and the utilization of CO_2. *Energy and Environmental Science* **2012**, *5*, 7281–7305

.

(11) Matuszewski, M.; Ciferno, J.; Marano, J. J.; Chen, S. *Research and Development Goals for CO_2 Capture Technology*; Department of Energy, 2011; Vol. December

.

(12) House, K. Z.; Baclig, A. C.; Ranjan, M.; Nierop, E. A. V.; Wilcox, J.; Herzog, H. J. Economic and energetic analysis of capturing CO_2 from ambient air. *PNAS* **2011**, *108*, 20428–20433

.

(13) Li, K.; Leigh, W.; Feron, P.; Yu, H.; Tade, M. Systematic study of aqueous monoethanolamine (MEA)-based CO_2 capture process: Techno-economic assessment of the MEA process and its improvements. *Applied Energy* **2016**, *165*, 648–659

926 .

927 (14) Jin, S.; Wu, M.; Gordon, R. G.; Aziz, M. J.; Kwabi, D. G. pH swing cycle for CO_2
928 capture electrochemically driven through proton-coupled electron transfer. *Energy and*
929 *Environmental Science* **2020**, *13*, 3706–3722

930 .

931 (15) Shaw, R. A.; Hatton, T. A. Electrochemical CO_2 capture thermodynamics. *Interna-*
932 *tional Journal of Greenhouse Gas Control* **2020**, *95*, 102878

933 .

934 (16) Boualavong, J.; Gorski, C. A. Electrochemically Mediated CO_2 Capture Using Aqueous
935 Cu(II)/Cu(I) Imidazole Complexes. *ACS ES&T Engineering* **2021**, *1*, 1084–1093

936 .

937 (17) Boualavong, J.; Papakonstantinou, K. G.; Gorski, C. A. Determining Desired Sor-
938 bent Properties for Proton-Coupled Electron Transfer-controlled CO_2 Capture using
939 an Adaptive Sampling-Refined Classifier. *Chemical Engineering Science* **2023**, *274*,
940 11873

941 .

942 (18) Millet, P. *Hydrogen Production: By Electrolysis*; Wiley-VCH, 2015; pp 167–190

943 .

944 (19) Gurkan, B.; Simeon, F.; Hatton, T. A. Quinone Reduction in Ionic Liquids for Elec-
945 trochemical CO_2 Separation. *ACS Sustainable Chemistry and Engineering* **2015**, *3*,
946 1394–1405

947 .

948 (20) Legrand, L.; Schaetzle, O.; Kler, R. C. D.; Hamelers, H. V. Solvent-Free CO_2 Cap-
949 ture Using Membrane Capacitive Deionization. *Environmental Science and Technology*
950 **2018**, *52*, 9478–9485

951 .

952 (21) Wang, M.; Hariharan, S.; Shaw, R. A.; Hatton, T. A. Energetics of electrochemically
953 mediated amine regeneration process for flue gas CO_2 capture. *International Journal*
954 *of Greenhouse Gas Control* **2019**, *82*, 48–58

955 .

956 (22) Rahimi, M.; Zucchelli, F.; Puccini, M.; Hatton, T. A. Improved CO_2 Capture Perfor-
957 mance of Electrochemically Mediated Amine Regeneration Processes with Ionic Sur-
958 factant Additives. *ACS Applied Energy Materials* **2020**, *3*, 10823–10830

959 .

960 (23) Rahimi, M.; Catalini, G.; Hariharan, S.; Wang, M.; Puccini, M.; Hatton, T. A. Carbon
961 Dioxide Capture Using an Electrochemically Driven Proton Concentration Process. *Cell*
962 *Reports Physical Science* **2020**, *1*, 100033

963 .

964 (24) Wang, C.; Jiang, K.; Yu, H.; Yang, S.; Li, K. Copper electrowinning-coupled CO_2
965 capture in solvent based post-combustion capture. *Applied Energy* **2022**, *316*, 119086

966 .

967 (25) Wang, C.; Jiang, K.; Jones, T. W.; Yang, S.; Yu, H.; Feron, P.; Li, K. Electrowinning-
968 coupled CO_2 capture with energy-efficient absorbent regeneration: Towards practical
969 application. *Chemical Engineering Journal* **2022**, *427*, 131981

970 .

971 (26) Caplow, M. Kinetics of Carbamate Formation and Breakdown. *Journal of the American*
972 *Chemical Society* **1968**, *90*, 6795–6803

973 .

974 (27) Watkins, J. D.; Siefert, N. S.; Zhou, X.; Myers, C. R.; Kitchin, J. R.; Hopkinson, D. P.;

975 Nulwala, H. B. Redox-Mediated Separation of Carbon Dioxide from Flue Gas. *Energy*
976 *and Fuels* **2015**, *29*, 7508–7515
977 .

978 (28) Huang, C.; Liu, C.; Wu, K.; Yue, H.; Tang, S.; Lu, H.; Liang, B. CO_2 Capture from Flue
979 Gas Using an Electrochemically Reversible Hydroquinone/Quinone Solution. *Energy*
980 *and Fuels* **2019**, *33*, 3380–3389
981 .

982 (29) Xie, H.; Wu, Y.; Wang, F.; Liang, B.; Chen, B.; Liu, T. Low-energy-consumption
983 electrochemical CO_2 capture driven by biomimetic phenazine derivatives redox medium.
984 *Applied Energy* **2020**, *259*, 114119
985 .

986 (30) Xie, H.; Jiang, W.; Liu, T.; Wu, Y.; Wang, Y.; Chen, B.; Niu, D.; Liang, B. Low-Energy
987 Electrochemical Carbon Dioxide Capture Based on a Biological Redox Proton Carrier.
988 *Cell Reports Physical Science* **2020**, *1*, 100046
989 .

990 (31) Simpson, T. C.; Durand, R. R. Reactivity of carbon dioxide with quinones. *Electrochim-*
991 *ica Acta* **1990**, *35*, 1399–1403
992 .

993 (32) Liu, Y.; Ye, H. Z.; Diederichsen, K. M.; Voorhis, T. V.; Hatton, T. A. Electrochemi-
994 cally mediated carbon dioxide separation with quinone chemistry in salt-concentrated
995 aqueous media. *Nature Communications* **2020**, *11*, 1–12
996 .

997 (33) Scovazzo, P.; Poshusta, J.; DuBois, D.; Koval, C.; Noble, R. Electrochemical Separation
998 and Concentration of <1*Journal of The Electrochemical Society* **2003**, *150*, D91
999 .

(34) Rahimi, M.; Diederichsen, K. M.; Ozbek, N.; Wang, M.; Choi, W.; Hatton, T. A. An Electrochemically Mediated Amine Regeneration Process with a Mixed Absorbent for Postcombustion CO_2Capture. *Environmental Science and Technology* **2020**, *54*, 8999–9007
.

(35) Stern, M. C.; Hatton, T. A. Bench-scale demonstration of CO_2 capture with electrochemically-mediated amine regeneration. *RSC Advances* **2014**, *4*, 5906–5914
.

(36) Welty, J.; Rorrer, G. L.; Foster, D. G. *Fundamentals of Momentum, Heat and Mass Transfer*, 5th ed.; Wiley, 2013
.

(37) Yu, C. H.; Huang, C. H.; Tan, C. S. A review of CO_2 capture by absorption and adsorption. *Aerosol and Air Quality Research* **2012**, *12*, 745–769
.

(38) Puxty, G.; Maeder, M. A simple chemical model to represent CO_2-amine-H_2O vapour-liquid-equilibria. *International Journal of Greenhouse Gas Control* **2013**, *17*, 215–224
.

(39) Jiang, Y.; Mathias, P. M.; Freeman, C. J.; Swisher, J. A.; Zheng, R. F.; Whyatt, G. A.; Heldebrant, D. J. Techno-economic comparison of various process configurations for post-combustion carbon capture using a single-component water-lean solvent. *International Journal of Greenhouse Gas Control* **2021**, *106*, 103279
.

(40) Hoyt, N. C.; Hawthorne, K. L.; Savinell, R. F.; Wainright, J. S. Plating Utilization of Carbon Felt in a Hybrid Flow Battery. *Journal of the Electrochemical Society* **2016**, *163*, A5041–A5048

.

(41) Etemad, E.; Ghaemi, A.; Shirvani, M. Rigorous correlation for CO2 mass transfer flux in reactive absorption processes. *International Journal of Greenhouse Gas Control* **2015**, *42*, 288–295

.

(42) Dutcher, B.; Fan, M.; Russell, A. G. Amine-based CO_2 capture technology development from the beginning of 2013-A review. *ACS Applied Materials and Interfaces* **2015**, *7*, 2137–2148

.

(43) Astarita, G. Regimes of Mass Transfer With Chemical Reaction. *Industrial & Engineering Chemistry* **1966**, *58*, 18–26

.

(44) van Krevelen, D. W.; Hoftijzer, P. J. Kinetics of gas-liquid reactions part I. General theory. *Recueil des Travaux Chimiques des Pays-Bas* **1948**, *67*, 563–586

.

(45) Shen, Y.; Jiang, C.; Zhang, S.; Chen, J.; Wang, L.; Chen, J. Biphasic solvent for CO_2 capture: Amine property-performance and heat duty relationship. *Applied Energy* **2018**, *230*, 726–733

.

(46) Kim, M.; Song, H. J.; Lee, M. G.; Jo, H. Y.; Park, J. W. Kinetics and steric hindrance effects of carbon dioxide absorption into aqueous potassium alaninate solutions. *Industrial and Engineering Chemistry Research* **2012**, *51*, 2570–2577

.

(47) van Holst, J.; Versteeg, G. F.; Brilman, D. W.; Hogendoorn, J. A. Kinetic study of CO_2

with various amino acid salts in aqueous solution. *Chemical Engineering Science* **2009**, *64*, 59–68

.

(48) Xiao, X. Q.; Li, K. On the Use of an Electrochemical Membrane Module for Removal of CO_2 from a Breathing Gas Mixture. *Transactions of the Institution of Chemical Engineers* **1997**, *75*, 438–446

.

(49) Shen, S.; Yang, Y. N.; Bian, Y.; Zhao, Y. Kinetics of CO_2 Absorption into Aqueous Basic Amino Acid Salt: Potassium Salt of Lysine Solution. *Environmental Science and Technology* **2016**, *50*, 2054–2063

.

(50) Zeman, F. Energy and material balance of CO_2 capture from ambient air. *Environmental Science and Technology* **2007**, *41*, 7558–7563

.

(51) Bishnoi, S.; Rochelle, G. T. Absorption of carbon dioxide into aqueous piperazine: Reaction kinetics, mass transfer and solubility. *Chemical Engineering Science* **2000**, *55*, 5531–5543

.

(52) Stolaroff, J. K.; Keith, D. W.; Lowry, G. V. Carbon Dioxide Capture from Atmospheric Air Using Sodium Hydroxide Spray. *Environmental Science and Technology* **2008**, *42*, 2728–2735

.

(53) Holmes, G.; Keith, D. W. An air-liquid contactor for large-scale capture of CO2 from air. *Philosophical Transactions of the Royal Society A: Mathematical, Physical and Engineering Sciences* **2012**, *370*, 4380–4403

.

(54) Pocker, Y.; Bjorkquist, D. W. Stopped-Flow Studies of Carbon Dioxide Hydration and Bicarbonate Dehydration in H_2O and D_2O. Acid-Base and Metal Ion Catalysis. *Journal of the American Chemical Society* **1977**, *99*, 6537–6543

.

(55) Couchaux, G.; Barth, D.; Jacquin, M.; Faraj, A.; Grandjean, J. Kinetics of carbon dioxide with amines. I. Stopped-flow studies in aqueous solutions. A review. *Oil and Gas Science and Technology* **2014**, *69*, 865–884

.

(56) Versteeg, G. F.; Dijck, L. A. V.; Swaaij, W. P. V. On the kinetics between CO_2 and alkanolamines both in aqueous and non-aqueous solutions. An overview. *Chemical Engineering Communications* **1996**, *144*, 133–158

.

(57) Khalili, F.; Rayer, A. V.; Henni, A.; East, A. L.; Tontiwachwuthikul, P. Kinetics and dissociation constants (pK_a) of polyamines of importance in post-combustion carbon dioxide (CO_2) capture studies. *ACS Symposium Series* **2012**, *1097*, 43–70

.

(58) Lvov, S. N. *Introduction to Electrochemical Science and Engineering*; CRC Press, 2012

.

(59) Thomas, W. J. Diffusion Coefficients in Strong Aqueous Amine Solutions. *Journal of Applied Chemistry* **1969**, *19*, 227–229

.

(60) Cheng, F. Y.; Li, D. Multiobjective Optimization Design with Pareto Genetic Algorithm. *Journal of Structural Engineering* **1997**, *123*, 1252–1261

.

(61) Huynh, M. T.; Anson, C. W.; Cavell, A. C.; Stahl, S. S.; Hammes-Schiffer, S. Quinone 1 e^- and 2 e^-/2 H^+ Reduction Potentials: Identification and Analysis of Deviations from Systematic Scaling Relationships. *Journal of the American Chemical Society* **2016**, *138*, 15903–15910
.

(62) Hikita, H.; Asai, S.; Ishikawa, H.; Honda, M. The kinetics of reactions of carbon dioxide with monoethanolamine, diethanolamine and triethanolamine by a rapid mixing method. *The Chemical Engineering Journal* **1977**, *13*, 7–12
.

(63) Liang, Y.; Liu, H.; Rongwong, W.; Liang, Z.; Idem, R.; Tontiwachwuthikul, P. Solubility, absorption heat and mass transfer studies of CO_2 absorption into aqueous solution of 1-dimethylamino-2-propanol. *Fuel* **2015**, *144*, 121–129
.

(64) Sada, E.; Kumazawa, H.; Butt, M. A. Gas absorption with consecutive chemical reaction: Absorption of carbon dioxide into aqueous amine solutions. *The Canadian Journal of Chemical Engineering* **1976**, *54*, 421–424
.

(65) Sartori, G.; Savage, D. W. Sterically Hindered Amines for CO_2 Removal from Gases. *Industrial and Engineering Chemistry Fundamentals* **1983**, *22*, 239–249
.

(66) Scrucca, L. GA: A Package for Genetic Algorithms in R. *Journal of Statistical Software* **2013**, *53*, 1–37
.

(67) Scrucca, L. On Some Extensions to GA Package: Hybrid Optimisation, Parallelisa-

tion and Islands EvolutionOn some extensions to GA package: hybrid optimisation, parallelisation and islands evolution. *The R Journal* **2017**, *9*, 187

.

(68) Binois, M.; Picheny, V. Gpareto: An r package for gaussian-process-based multi-objective optimization and analysis. *Journal of Statistical Software* **2019**, *89*, 1–30

.

(69) Lin, Y. J.; Chen, E.; Rochelle, G. T. Pilot plant test of the advanced flash stripper for CO_2 capture. *Faraday Discussions* **2016**, *192*, 37–58

.

(70) Puxty, G.; Rowland, R.; Allport, A.; Yang, Q.; Bown, M.; Burns, R.; Maeder, M.; Attalla, M. Carbon dioxide postcombustion capture: A novel screening study of the carbon dioxide absorption performance of 76 amines. *Environmental Science and Technology* **2009**, *43*, 6427–6433

.

(71) Richner, G.; Puxty, G.; Carnal, A.; Conway, W.; Maeder, M.; Pearson, P. Thermokinetic properties and performance evaluation of benzylamine-based solvents for CO_2 capture. *Chemical Engineering Journal* **2015**, *264*, 230–240

.

(72) Datta, S.; Henry, M. P.; Lin, Y. J.; Fracaro, A. T.; Millard, C. S.; Snyder, S. W.; Stiles, R. L.; Shah, J.; Yuan, J.; Wesoloski, L.; Dorner, R. W.; Carlson, W. M. Electrochemical CO_2 capture using resin-wafer electrodeionization. *Industrial and Engineering Chemistry Research* **2013**, *52*, 15177–15186

.

(73) Clarke, L. E.; Leonard, M. E.; Hatton, T. A.; Brushett, F. R. Thermodynamic Modeling

of CO_2 Separation Systems with Soluble, Redox-Active Capture Species. *Industrial and Engineering Chemistry Research* **2022**, *61*, 10531–10546
.

(74) Friedman, J. H. Greedy Function Approximation: A Gradient Boosting Machine. *The Annals of Statistics* **2001**, *29*, 1189–1232
.

(75) Zhao, B.; Liu, F.; Cui, Z.; Liu, C.; Yue, H.; Tang, S.; Liu, Y.; Lu, H.; Liang, B. Enhancing the energetic efficiency of MDEA/PZ-based CO_2 capture technology for a 650 MW power plant: Process improvement. *Applied Energy* **2017**, *185*, 362–375
.

(76) Liaw, A.; Wiener, M. Classification and Regression by randomForest. *R News* **2002**, *2*, 18–22
.

(77) Sharifian, R.; Wagterveld, R. M.; Digdaya, I. A.; Xiang, C.; Vermaas, D. A. Electrochemical carbon dioxide capture to close the carbon cycle. *Energy and Environmental Science* **2021**, *14*, 781–814
.

(78) Rubio-Garcia, J.; Kucernak, A.; Parra-Puerto, A.; Liu, R.; Chakrabarti, B. Hydrogen/functionalized benzoquinone for a high-performance regenerative fuel cell as a potential large-scale energy storage platform. *Journal of Materials Chemistry A* **2020**, *8*, 3933–3941
.

(79) Dargily, N. C.; Thimmappa, R.; Bhat, Z. M.; Devendrachari, M. C.; Kottaichamy, A. R.; Gautam, M.; Shafi, S. P.; Thotiyl, M. O. A Rechargeable Hydrogen Battery. *The Journal of Physical Chemistry Letters* **2018**, *9*, 2492–2497

.

(80) Crawford, A.; Viswanathan, V.; Stephenson, D.; Wang, W.; Thomsen, E.; Reed, D.; Li, B.; Balducci, P.; Kintner-Meyer, M.; Sprenkle, V. Comparative analysis for various redox flow batteries chemistries using a cost performance model. *Journal of Power Sources* **2015**, *293*, 388–399

.

(81) Soloveichik, G. L. Flow Batteries: Current Status and Trends. *Chemical Reviews* **2015**, *115*, 11533–11558

.

(82) McCann, N.; Phan, D.; Wang, X.; Conway, W.; Burns, R.; Attalla, M.; Puxty, G.; Maeder, M. Kinetics and mechanism of carbamate formation from CO_2(aq), carbonate species, and monoethanolamine in aqueous solution. *Journal of Physical Chemistry A* **2009**, *113*, 5022–5029

.

(83) Puxty, G.; Rowland, R. Modeling CO_2 mass transfer in amine mixtures: PZ-AMP and PZ-MDEA. *Environmental Science and Technology* **2011**, *45*, 2398–2405

.

(84) Liu, Y.; Lucas, E. O.; Sullivan, I.; Li, X.; Xiang, C. iScience Challenges and opportunities in continuous flow processes for electrochemically mediated carbon capture. *iScience* **2022**, *25*, 105153

.

TOC Graphic

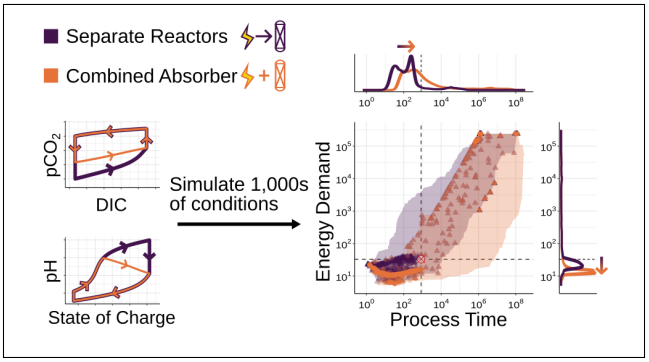
Separate Reactors
Combined Absorber
pCO2
DIC
pH
State of Charge
Simulate 1,000s
of conditions
Energy Demand
Process Time